MODELING OF MULTIBODY DYNAMICS IN FORMULA SAE VEHICLE SUSPENSION SYSTEMS

A Thesis

Submitted to the Faculty

of

Purdue University

by

Swapnil Pravin Bansode

In Partial Fulfillment of the

Requirements for the Degree

of

Master of Science in Mechanical Engineering

May 2020

Purdue University

Indianapolis, Indiana

THE PURDUE UNIVERSITY GRADUATE SCHOOL
STATEMENT OF THESIS APPROVAL

Dr. Jing Zhang, Chair

Department of Mechanical and Energy Engineering

Dr. Hamid Dalir

Department of Mechanical and Energy Engineering

Dr. Lingxi Li

Department of Electrical and Computer Engineering

Approved by:

Dr. Jie Chen

Head of the Graduate Program

Dedicated to loving memory of my mother and grandmother.

ACKNOWLEDGMENTS

I would like to express sincere gratitude to my advisor Dr. Jing Zhang for providing guidance and being an incredible source of knowledge throughout my research work. I would like to thank members of advisory committee, Dr. Hamid Dalir and Dr. Lingxi Li for sharing their thoughts and feedback which helped me broaden my perspective of research work. I would also like to thank Mr. Jerry Mooney for his valuable inputs for my thesis.

I would like to thank IUPUI and entire staff of Department of Mechanical and Energy Engineering for providing support and assistance during various stages of my research. I would also like to thank my lab mates Tejesh, Harshal, Michael Golub, Jian, Xuehui and Lingbin for their support.

Lastly, I would like to thank my aunt and all my family, for supporting me both financially and emotionally , along with my friends, Madhura, Tripthi, Jay, Fermin, Sailee and Riddhi for always being with me throughout my graduate journey.

TABLE OF CONTENTS

Page

Page

LIST OF TABLES

LIST OF FIGURES

Figure Page

Figure Page

SYMBOLS

K_S	Spring rate
K_W	Wheel rate
K_{ϕ_F}	Front roll rate (Nm/deg)
K_{ϕ_R}	Rear roll rate (Nm/deg)
η_L	Longitudinal dynamic caster
η_S	Lateral dynamic caster
F_{Z^0}	Nominal vertical force
l_0, l_1	Caster parameter
l_F	Front base length
b_F	Front track length
δ_W	Steering angle for wheel
r	Distance of tire from center
α	Vehicle side slip angle
s_L	Longitudinal slip
s_S	Lateral slip
v_R	Desired direction of vehicle velocity
v_W	Actual direction of vehicle velocity
β	Desired direction for vehicle
$\dot{\psi}$	Yaw rate
α_F	Front tire side slip angle
α_R	Rear tire side slip angle
μ_L	Longitudinal frictional coefficient
μ_S	Lateral frictional coefficient
m_S	Sprung mass

m_{US}	Unsprung mass
M_ϕ	Rolling moment
W_S	Sprung weight
Z_{RC}	Roll center height
A_y	Centripetal acceleration
K_ϕ	Roll stiffness

ABBREVIATIONS

FS	Formula student
SAE	Society of Automotive Engineers
MBD	Multibody dynamics

ABSTRACT

Bansode, Swapnil P. M.S.M.E., Purdue University, May 2020. Modeling of Multibody Dynamics in Formula SAE Vehicle Suspension Systems. Major Professor: Jing Zhang.

Indiana University–Purdue University Indianapolis student team Jaguar has been participating in the electric Formula SAE (FSAE) vehicle competitions in the past few years. There is an urgent need to develop a design tool for improving the performance of the vehicle. In this thesis, multibody dynamics (MBD) models have been developed which allow the student team to improve their vehicle design, while reducing the required time and actual testing costs. Although there were some studies about MBD analyses for vehicles in literature, a detailed modeling study of key parameters is still missing. Specifically, the effect of suspension system on the vehicle performance is not well studied. The objective of the thesis is to develop an MBD based model to improve the FSAE vehicle's performance. Based on the objective and knowledge gap, the following research tasks are proposed: (1) MBD modeling of current suspension systems; (2) Modification of suspension systems, and (3) Evaluation of performance of modified suspension systems. The models for the front suspension system, rear suspension system, and full assembly are created, and a series of MBD analyses are conducted. The parameters of the vehicle by conducting virtual tests on the suspension model and overall vehicle model are studied. In this work, two main virtual tests are performed. First, parallel wheel travel test on suspension system, in which the individual suspension system is subject to equal force on both sides. The test helps understand the variation in stability parameters, such as camber angle, toe angle, motion ratio, and roll center location. Second, skid-pad test on full assembly of the vehicle. The test assists in understanding the vehicle's behavior in constant

radius cornering and the tire side slip angle variation, as it is one of the important parameters controlling alignment of the vehicle in this test. Based on the vehicle's dynamics knowledge obtained from the existing vehicle, a modified version of the FSAE vehicle is proposed, which can provide a better cornering performance with minimum upgrades and cost possible. Based on the results from the parallel wheel travel test and skid-pad test, the lateral load transfer method is used to control the vehicle slip, by making changes to the geometry of the vehicle and obtaining appropriate roll center height for both front and rear suspension system. The results show that the stiffness in front suspension system and rear suspension system are controlled by manipulating roll center height. This study has provided insightful understanding of the parameters and forces involved in suspension system and their variations in different events influencing vehicle stability. Moreover, the MBD approach developed in this work can be readily extended to other commercial vehicles and sports vehicles.

1. INTRODUCTION

1.1 Formula SAE and formula hybrid vehicles

Conceived by Dr. Kurt M. Marshek, SAE Mini-Indy was held at the University of Houston in 1979. In 1980, as the Mini-Indy died, a group of student members in SAE came together to form a new collegiate group in which students can apply the concepts learned in the classroom to real life and build a car. Thus, Formula SAE started with student members in SAE collegiate club under the guidance of Prof. Matthews and he came up with the name 'Formula SAE'.

The main objective of the FSAE competition is to design and build a student formula race car which is complaint with all the safety rules. The car once build is evaluated as production item by analyzing its overall cost and innovations. FSAE competition mainly focuses on two objectives. First to design a formula style car ensuring all the safety possible on track and second, innovative solutions for the given problems. Various sponsors of the competition provide awards for superior design accomplishments. For example, best use of E-85 ethanol fuel, innovative use of electronics, recyclable, crash worthiness, analytical approach to design, and overall dynamic performance are some of the awards available. Before the competition, the vehicle is checked for rule compliance during the Technical Inspection. Its braking ability, rollover stability and noise levels are checked before the vehicle is allowed to compete in the dynamic events (Skidpad, Autocross, Acceleration, and Endurance). Formula SAE provides engineering education by allowing students to apply their skills and creativity to build a car with enhanced performance parameters and, also, considering all the safety norms. From [1] and [2], the rules can be summarized as:
Competition: Teams are expected to design, build, test and demonstrate a prototype formula like vehicle. Teams are also expected to do everything mentioned on their

own without any help from professionals. Teams can be advised by a third person or professional but in the end the team is supposed to design and fabricate the vehicle on their own.

Engine: Two main Engine limitations are, first, the engine should be four stroke primary heat cycle engine. Second, total combined displacement of the engine must be equal to or less than 710 cc. For FSAE, hybrid power trains are strictly prohibited. Although, lost or waste heat can be converted and stored. Rules do not restrict teams from building an engine from scratch. But most teams consider using motorcycle engines which can give up to 600 cc displacement.

Suspension: Suspension system is required to be on the vehicle, both in front and back, with shock absorbers. The suspension system is also required to be designed in such a way that the wheel travel of minimum of 50 mm can be achieved (in case of bump and droop). Failure to comply with this and not able to provide appropriate handling characteristics for the vehicle can result in disqualification.

Aerodynamics: Most teams do not consider designing and installing aerodynamic packages as the speed in FSAE never exceeds more than 97 km/hr. Although some teams do go for aerodynamic design and expected to provide extensively accurate data from the test such as wind tunnel tests and computational fluid dynamics.

Weight: According to the rules of 2019, there is no restriction for weight of the car. Although, teams are coming up with innovative solutions to reduce the weight of the car as much as possible. Usually the weight of the car is in the range of 200 - 300 kg. Even if there are no restrictions or points for weight reduction, fuel economy plays an important role in endurance tests.

Safety: One of the main objectives in FSAE is to design safety of the car. The vehicle is required to have an impact attenuator at the front to absorb the energy of impact on collision. The shape of roll hoops both on front and back are mentioned in the rules with the required dimensions. Rules also require for two fire extinguishers to be mounted on the vehicle for fire safety along with a 5 point belt.

Formula SAE hybrid can be considered as a branch rooted out from FSAE. In 2007, Formula SAE hybrid was started at Thayer School of Engineering and Technology at Dartmouth College. Along with the requirements of FSAE, FSAE hybrid focuses on drivetrain and fuel efficiency improvisation with innovative ideas. With the challenges of FSAE, this competition adds an extra challenge of coming up with hybrid technology for the vehicle. Rules for Formula Hybrid are based on FSAE rules along with additional and specific rules for Hybrid powertrain. One of the main differences in both competitions is that the FSAE hybrid has an acceleration event where the vehicle is supposed to accelerate on a 75 m long track within just 10 seconds. As far as engine specification is considered, an ignition engine with 250 cc displacement and diesel engine with 310 cc displacement is required. From [1], the limitation on accumulator capacity is explained in the table below.

Table 1.1.
Limitation on accumulator capacity

Hybrid vehicle	
Endurance Energy Allocation	31.25 MJ
Maximum Accumulator Capacity	4,449 Wh
Electric Vehicle	
Maximum Accumulator	5400 Wh

To qualify as a hybrid, vehicles must have a drive system utilizing one or more electric motors with a minimum continuous power rating of 2.5 kW (sum total of all motors) and one or more I.C engines with a minimum (sum total) power rating of 2.5 kW.

1.2 Multibody dynamics

A multibody simulation, in general, can be divided into 6 steps [1]. The very first step is to create a geometric model which is required for a desired purpose. For

example, a gear mechanism is created in any 3D modeling software. Designing a gear in 3D modeling software gives us a perspective of how the model is supposed to be and can help us or the engineer who is supposed to work on dynamics of that particular mechanism. Second step is to transfer data from the model to the Dynamics software. The gear mechanism can be a part of a bigger mechanism. In order to get exact values, it is necessary to find the dimensions of the gear which can easily be done from the 3D model. It is possible to connect some 3D softwares to the dynamics software but in some cases, this transfer has to be done manually coordinate by coordinate. This brings us to the third step, building a dynamic model in software. This can be the most complex step depending upon the mechanism and available information for the model. 3D model data transfer can be insufficient in some cases and you need to know all the coordinates of the model so that you can make corrections in the data interpreted from the 3D model by the software or you have to create coordinates from scratch. Fourth step is to give boundary conditions to the model, such as giving input for force, velocity, acceleration, moments etc. Fifth step is to simulate the given mechanism after providing the input and boundary conditions. For simulations, solver is the heart of any simulation software. A solver consists of a set of algorithms which when given a specific input provides the final result for that mechanism predicting the behavior of the mechanism. This is the sixth step of the simulation, analysis and prediction [1]. From the results, the behavior of the system is analyzed and checked if the desired operation is possible or not. If not what are the parameters that are going through undesired changes and how they can be improved or optimized .

The solver base for the equations is formulated from Newton's Law of motion which leads to various approaches such as Newton-Euler formulation and Lagrange-Kane formulation [2]. The Newton-Euler formulation consists of all constraint forces acting on the bodies of the system under study. This results in getting more unknown equations than known variables. Lagrange-Kane formulation eliminates this problem by using d'Alembert's principle which reduces the number of equations which in turn reduces computational time.

The vehicle under study is a FSAE vehicle designed and fabricated by Team Jaguars, IUPUI. All the data pertaining to the vehicle is extracted from the 3D model of the vehicle available with the team. All the forces, velocities, moments and other constraints are decided based on reference from [3] and some other reference papers. Some parameters are also assumed based on availability of data and calculations and eliminate errors in simulations. Multibody dynamics can be studied for as simple as 4 bar mechanisms to complicated suspension geometry. The more complex the system more the number of equations are involved [2]. The equations related to this study are mentioned and discussed below in the respective sections and the results obtained from the MBD solver are used to predict the nature and behavior of the system pointing towards the handling and rider's comfort. The equations in the solver range from Newton's Law of motion to Newton Euler Law to Kane's formulation depending upon the complexity of the system. More information about FSAE and its rules and regulations is provided in the upcoming sections and their role in the test carried out on the vehicle.

1.3 Motivation

Fig. 1.1. Present IUPUI Jaguar FSAE vehicle

In the 1980's, computer based analysis for understanding dynamics in machinery started developing along with the Finite Element Analysis in industries [3]. All types

of design and dynamics engineers started using these programs, also known as Multibody Dynamics of systems for studying behaviors of dynamic motion in machines. Unlike FEA, MBD simulations consist of bodies connected using joints and resultant motion when external forces act on it.

Multibody Simulations are numerical solutions for multibody systems which are connected to each other by rigid and elastic bodies. A multibody system usually consists of kinematic constraints as connections such as joints and force elements such as spring damper. Friction can also be introduced in the design of the multibody system.Multibody simulation has become very important for motion analysis when it comes to product development to evaluate the characteristics such as comfort and safety [4].

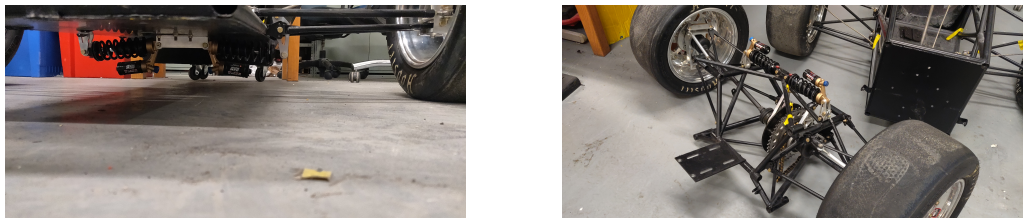

(a) Front (b) Rear

Fig. 1.2. Spring-damper location in the FSAE vehicle

MBD simulation is primarily used by the Automotive industry, following which came many industries such as electromechanical, agricultural, construction and aerospace industry [5]. Today, MBD can work on future designs and existing machinery to obtain resultant motion of the system designed and analyze the accuracy of the desired output. In some cases, designed prototypes can be subjected to extreme conditions and damage of such a prototype can result in loss of valuable time and money. Such designs can be programmed and simulated using the MBD methodology to find flaws in the design and analyze the result of the particular prototype [6]. MBD methodology can also be used to reverse engineer a particular system to find out the flaw in the system or reason due to which the system is behaving in a particular man-

ner. These reasons can include a crash of a vehicle or any mechanical system. In the automotive industry, MBD simulations are mainly used for analyzing suspension and steering systems to understand performance characteristics of a Vehicle when put through different conditions. MBD methodology is becoming more and more popular with the manufacturers so that the expensive build and test of the vehicles can be avoided. With development in MBD simulation software, it has now become possible to carry out different vehicle settings in different conditions while keeping check on financial constraint [7]

1.4 Knowledge gap

Suspension system analysis has played an important role in maintaining the stability of the vehicle. To understand the factors responsible for the stability of the vehicle, detailed study of all the suspension parameters is essential and literature review below shows the detailed study of these parameters. Along with the parameters studied, it is also essential to understand their nature and variation to predict the nature of the vehicle when it is subjected to external force. Force and moments acting on the vehicle tend to create instability, causing variation in suspension parameters [8]. Events like Cornering are crucial in this case as the vehicle experiences forces which can lead the vehicle to roll over or move out of track especially in Formula 1 cars, where controlling the vehicle during cornering is much more difficult as the vehicle is operated at higher speeds. Study and understanding suspension all together is crucial for such an event [9]. Thus, in this thesis, Multibody dynamics of an FSAE vehicle is conducted to understand the parameters of suspension system in static conditions and the behavior of the vehicle during cornering test. From initial results, vehicle behavior is predicted and a modified computational model for the vehicle is proposed.

1.5 Objective of thesis

The objective of the thesis is to develop an MBD based model to understand and improve the FSAE vehicle's performance. By going through extensive literature review and the problems given, the following research tasks are proposed:

1. **MBD modeling of the current suspension system:** Based on the vehicle dimensions and CAD model available, as first step of MBD, model is created and subjected to normal force. In this case, both front suspension system and rear suspension system are subjected to normal force.

2. **Full vehicle test:** Both the front and rear suspension system model created are now combined to understand their combined effect on the vehicle handling.

3. **Modification of suspension system:** Based on the effect on the vehicle both front and rear suspension system are subjected to modification. The primary aim is to focus on motion ratio and roll center location in both system

4. **Evaluation of performance of modified suspension system:** After modification, the suspension system is then tested for similar test and then combined to observe the behavior of the vehicle

1.6 Structure of thesis

This work has been divided in 8 parts. The first chapter consists of introduction which covers background of thesis including motivation, knowledge gap and objective of this work. The second chapter consists of literature review which covers basic definitions of the parameters essential to understand suspension system and its behavior. The third chapter is example study of McPherson strut suspension system to understand MBD software and its test parameters. The fourth chapter is the main testing of current model of FSAE vehicle model consisting of both parallel wheel travel test and skidpad test to observe vehicle handling performance. The fifth and

sixth chapter consists of wheel model and suspension model equations based on which the modifications in the suspension system are made. The seventh chapter explains modification in the suspension model and consists of test of front and rear suspension system and skid pad test to observe changes vehicle handling performance due to modifications. The eighth chapter concludes the work by summarizing the overall research and explaining limitations faced during testing.

2. LITERATURE REVIEW

In Formula 1, the vehicles are designed and built to participate in the races which require the highest level of performance along with controllability to ensure maximum speed at cornering and safety pilot [10]. Engineers working on F1 have to consider all kinds of forces acting on the vehicle during such events and then study to solve the additional tasks associated with performance, stability and safety [10].

When a car turns, there are forces acting on the car which can lead to negative results or can cause roll of the car. In order to study these parameters, which can lead to undesired results, understanding of the tire characteristics and suspension kinematics is very important [11]. Thus, to begin with model, understanding of parameters is essential and will be discussed in detail now.

Since the vehicle under study is FS car (i.e. Formula Student or Formula Style), unequal length A-arm wishbones are used, as in most race cars A-arm wishbones are used [12]. With use of A-arms, properties of the suspension system are associated. Thus, with the help of [12] the suspension properties are defined below:

2.1 Suspension system parameters

2.1.1 Camber angle

When a vehicle sits on the road, the tire is not vertical. Thus the angle at which the tire is tilted in-ward or outward is called camber angle of the vehicle. The angle is considered as positive camber if the tire is tilting outward or pointing outward, i.e., away from the vehicle and the angle is considered negative camber when the tire is pointing inward, i.e., towards the vehicle. In race cars, the camber angle used is always negative. There are some examples which used positive camber but the

race didn't end very well for them [3]. A negative camber provides grip by providing camber gain which in turn increases grip of the tire and provides high speed stability. Thus in the figure below, camber angle is shown.

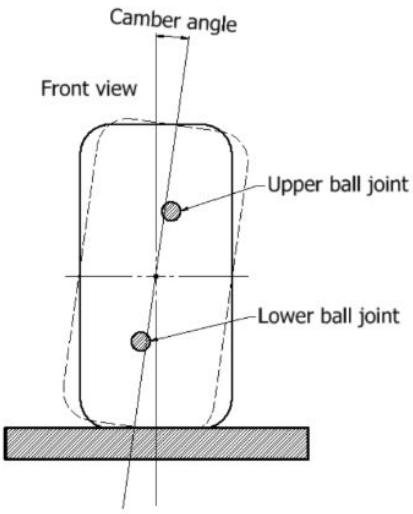

Fig. 2.1. Camber angle [12]

2.1.2 Caster angle

With reference to the above figure, the angle made by the steering axis between upper ball joint and lower ball joint when viewed from side is called Caster angle. The distance between the point where the steering axis touches the ground and the central axis of tire is called mechanical trail. A caster angle is considered positive when the mechanical trail is behind steering axis and is considered negative when the mechanical trail is in front of the steering axis. In race cars, positive caster is preferred as negative caster tends to make the car unstable when it comes to cornering.

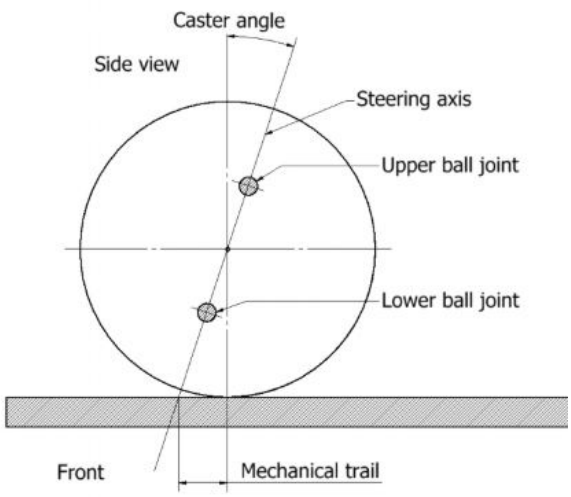

Fig. 2.2. Caster angle [12]

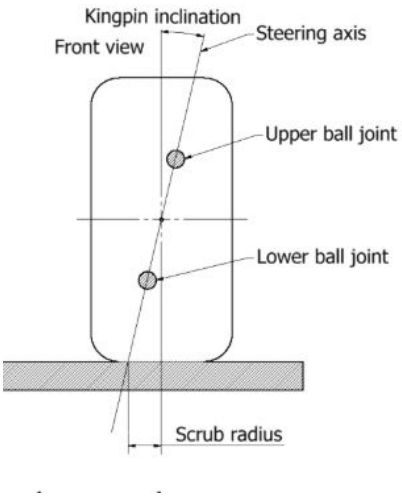

Fig. 2.3. Kingpin inclination [12]

2.1.3 Kingpin inclination

The angle made by steering axis, when it passes through the upper ball joint or upper outer joint and lower ball joint or lower outer joint, with the vertical is called Kingpin Inclination. When a car is in cornering, kingpin influences the lift of the car by lifting the car during cornering and by making the steering the straight as the

weight transfer returns back to its center. According to [13], if the kingpin axis passes through the vertical axis of tire, maximum stability can be achieved, however, this is not possible during actual practice. A kingpin inclination also affects camber angle as the wheel gains positive camber and can help in vehicle stability.

2.1.4 Scrub radius

From figure 2.3 the kingpin axis touches the ground at a certain distance from the vertical axis of the wheel. This distance is called scrub radius. In figure 2.3 The scrub radius is outside of the tire and is considered as negative. If the scrub radius is inside the tire toward the vehicle it is considered positive. The scrub radius can affect the toe of the tire as longitudinal forces act on the lever arm created due to scrub radius.

2.1.5 Wheel rate

Wheel Rate is defined as normal Force per unit length displacement of the center of the wheel and is the spring rate measured instead at spring. Wheel Rate is very important parameter when it comes to designing suspension parameters. A change in wheel rate changes the normal force acting on the wheel which in turn changes the lateral force acting on the wheel which is very important for stability measurement of the car. Spring rate is calculated by dividing the force by the length of spring displacement. Therefore, its equation is given as [12]:

$$K_S = F/l \tag{2.1}$$

where,

$$K_S = \textit{Spring Rate (N/m)}$$
$$F = \textit{Force acting on Spring (N)}$$
$$l = \textit{Spring Displacement (m)}$$

Motion ratio is given as displacement of spring divided by the displacement of center wheel (i.e. wheel displacement). Therefore, we have,

$$MR = (SpringTravel)/(WheelTravel) \tag{2.2}$$

Thus, the wheel rate is given by product of spring rate and square of motion ratio.

$$K_W = K_S * (MR)^2 \tag{2.3}$$

where,

$$K_W = Wheel\ Rate$$

The frequency equation for sprung mass system can be given as,

$$f = \frac{1}{2\pi} * \sqrt{\frac{K_s}{M}} \tag{2.4}$$

where,

$$f\ is\ frequency\ (Hz)$$

In the frequency equation, wheel rate and tire rate can be introduced and the equation can be given as,

$$f_s = \frac{1}{2\pi} * \sqrt{\frac{(K_w)(K_T)/(K_w + K_T)}{M_s}} \tag{2.5}$$

where,

f_s = *Natural frequency of sprung mass system*

K_W = *Wheel rate*

M_S = *Sprung mass*

And, the frequency of unsprung mass is given as,

$$f_{u_s} = \frac{1}{2\pi} * \sqrt{\frac{K_w + K_T}{M_{u_s}}} \tag{2.6}$$

2.1.6 Roll center height and roll rate

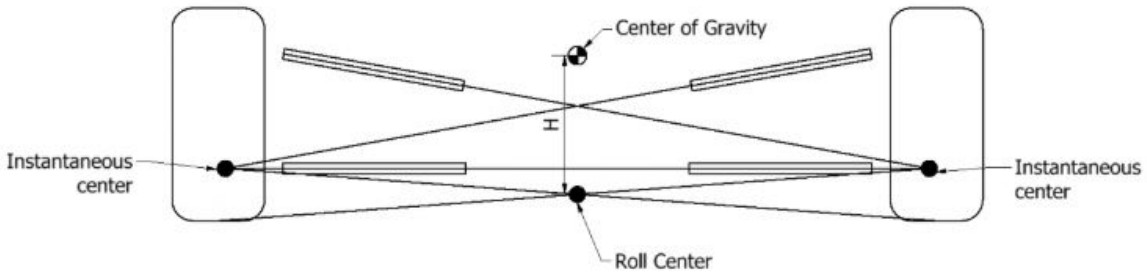

Fig. 2.4. Roll center location [12]

The distance of the point from the ground along which the vehicle tends to roll when lateral force applied on CoG is called Roll center height. Roll center can be found by connecting instantaneous centers of upper and lower wishbones to the ground contact point. The more the distance between CoG and Roll center, the more roll moment acts on it [14]. This moment is opposed by roll rate to keep the car stable. This stiffness can be calculated by calculating roll gradient.

Therefore, the roll gradient can be given as [12],

$$\frac{\phi_R}{A_y} = \frac{M * H}{K_{\phi_F} + K_{\phi_R}} \tag{2.7}$$

where,

A_y = *lateral acceleration (g)*

H = *Roll Center Height (m)*

M = *Mass of Vehicle (kg)*

K_{ϕ_F} = *Front roll rate (Nm/deg)*

K_{ϕ_R} = *Rear roll rate (Nm/deg)*

$$K_{\phi_F} = \frac{\pi * (t_f^2) * K_{L_F} * K_{R_F}}{180 * (K_{L_F} + K_{R_F})} \tag{2.8}$$

$$K_{\phi_R} = \frac{\pi * (t_r^2) * K_{L_R} * K_{R_R}}{180 * (K_{L_R} + K_{R_R})} \tag{2.9}$$

where,

t_f = *Front track width (m)*

t_r = *Rear track width (m)*

K_{L_F} = *Left front wheel rate (N/m)*

K_{R_F} = *Right front wheel rate (N/m)*

K_{L_R} = *Left rear wheel rate (N/m)*

K_{R_R} = *Right rear wheel rate (N/m)*

According to [12], the roll stiffness gradient should be in the range of 0.2 to 0.7/deg. If roll stiffness is not enough, anti-roll bars need to be installed. Thus, the total anti-roll bar stiffness needed to increase stiffness of car is given by,

$$K_\phi = K_{\phi_F} + K_{\phi_R} \tag{2.10}$$

$$K_{\phi_A} = \frac{\pi}{180} * (\frac{K_{\phi_d} * K_T * (t_A^2/2)}{K_T(t_A^2) * \pi/180 - K_{\phi_d}} \tag{2.11}$$

where,

K_{ϕ_A} = *Total anti-roll rate needed (N/m)*

K_{ϕ_d} = *desired total amount of roll stiffness (N/m)* t_A = *Average track (m)*

3. EXAMPLE OF MCPHERSON STRUT SUSPENSION SYSTEM

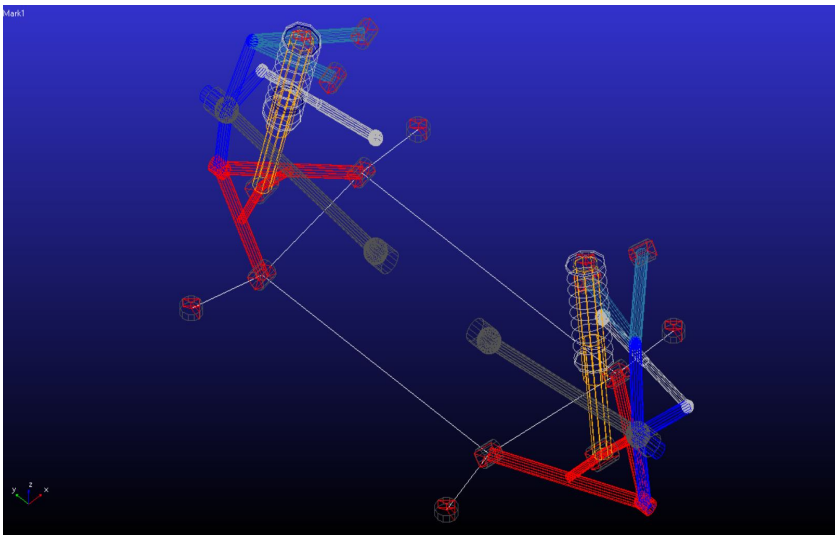

Fig. 3.1. McPherson strut wire suspension model

To study the general characteristics of an MBD model, an example involving McPherson strut suspension is used. The number of coils for this suspension is 9 in both right and left and is directly connected from lower wishbone to the chassis. Even though this suspension gives motion ratio 1 or close to 1, this is not normally used in Formula student but is used in heavy duty competitions like SAE Baja where this suspension is put to test using varying rough path. Suspensions used in FSAE are usually stiffer than the McPherson strut since the trail for FS is pretty straight without any huge obstacles. Intention of this example is to solely study the behavior of suspension using test rig. The model for test can be seen in figure 3.1 and 3.2 in both its wire structure and solid form. For running test on the mode, the model must be first assembled by calling in tires for the mechanism and test rig. In the test, force

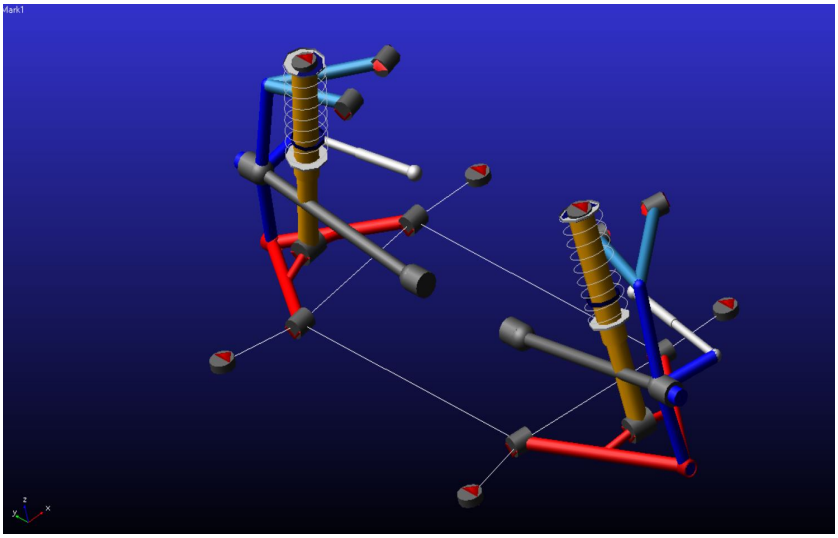

Fig. 3.2. McPherson strut solid suspension model

is applied from the bottom of the tires using test rig and the default force is chosen for this test i.e. 3000 N. For this test, the constraints we have to provide is wheel travel, step size and duration of test. Wheel travel for this test is taken as 100 mm, step size as 0.05 and duration of test 100 seconds. Along with constraints there is one more parameter important for suspension behavior, that is, hardpoints. All the hardpoints in the entire suspension system can be modified and set according to individual needs. Although, the points should be accurately placed as their improper placing can cause mechanism to intersect and failure. For this test, hardpoints are considered from default setting. Results after the test can be seen in the post-processor window which can be viewed with animation to observe the behavior of the system.

Results:

Wheel rate is basically stiffness of the tire and changes with the magnitude of force applied. In test, initial position of tire is at the bottom point, i.e. at -100 mm. From that position, constant force is applied on the tires until the top point 100 mm is reached. From figure 7, wheel stiffness at -100 mm position seems to around 25 N/m. Even though, the wheel reaches 20 mm, there is a very small change in tire stiffness and it continues to be under 30 N/m until it reaches 20 mm displacement

of the wheel. After 20mm, the stiffness droops to approximate stiffness of 12.5 N/m and then rises gradually upto 137 N/m and tire displacement from 30 mm to 60 mm. After this, the stiffness again droops to 120 N/m and then keeps on increasing.

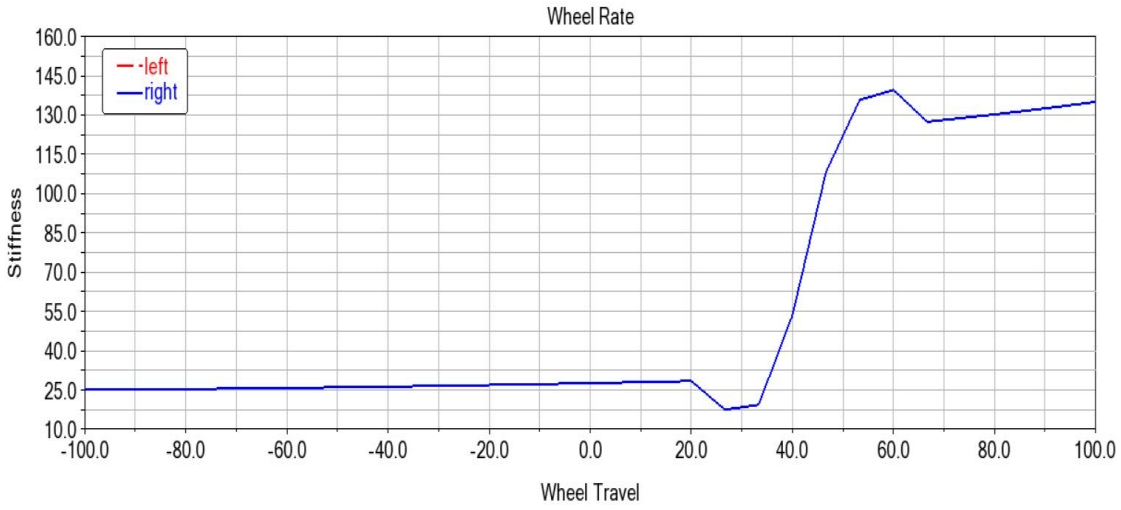

Fig. 3.3. Wheel rate

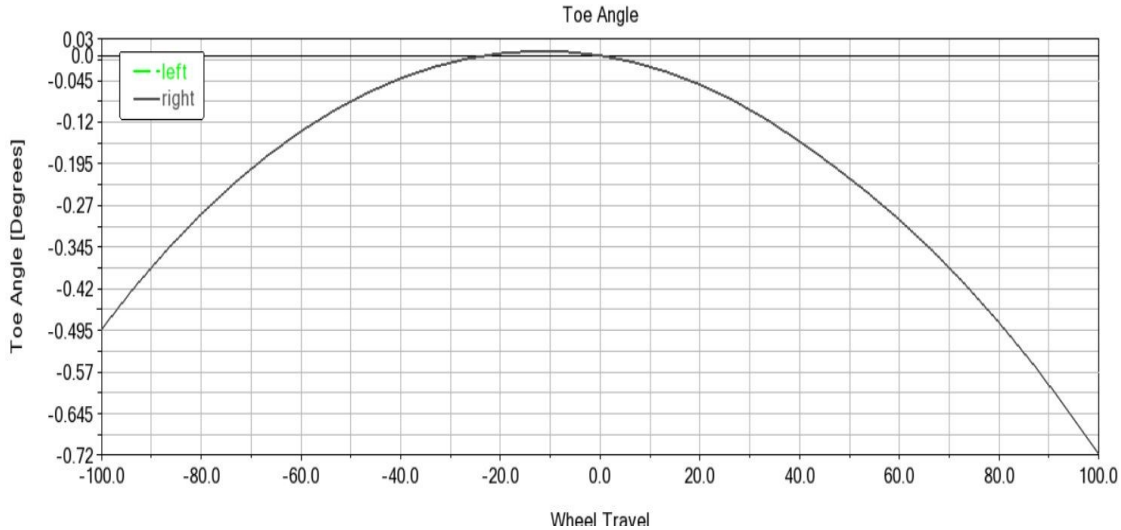

Fig. 3.4. Toe variation

When viewed from the top, in race cars, both front tires tend to pointed towards the longitudinal axis of the vehicle. The angle of inclination is toe angle of the car.

From graph in figure 3.4 we can see the behavior of the toe as it rises from negative to positive as the wheel travels from negative 100m to positive 100 mm. The angle is maximum at -10 mm travel and then again goes back to negative. For stability, toe angle is aimed to be negative. In positive case, the toe angle would tilt outwards, away from the vehicle's longitudinal axis which can lead to vehicle to destabilize during acceleration. From this figure, it can be observed that the tires are pointing inwards and move away from the axis as the tire rises but then after -10mm wheel travel, the tire goes back to pointing inwards, which in this case can be considered stable.

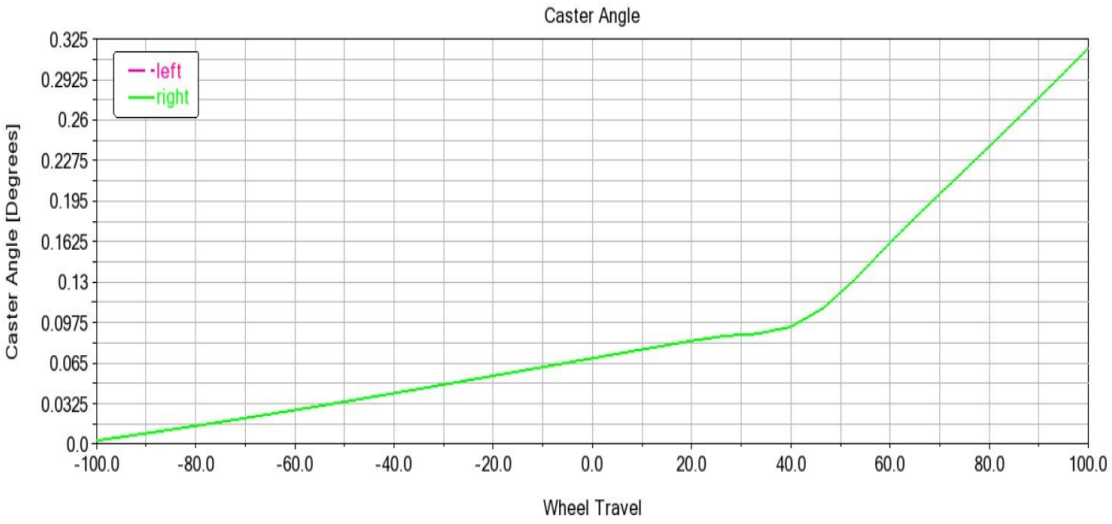

Fig. 3.5. Caster variation

When the wheel is at the bottomest point in this test, the caster angle is 0. With the wheel travel, the caster angle seems to increase gradually till 40mm after which increases exponentially. With increased caster angle, the mechanical trail also increases which provides steering with more self aligning moment.

Even after providing a static camber to the vehicle, the length of the A-arms connected to the upright holding the tire play a major role. In this case, since the upper arm holding the tire is shorter than the lower arm, the wheel tends to incline towards center at the bottom position. As the wheel rises during the test, it tends

to re-align itself with its vertical axis and keeps on going until the wheel reaches displacement of 42-45mm after which it tends to decrease and go back to negavtive value after 60mm. As the camber value stays in negative range for wheel travel of -100mm to approx 40mm during the test, the camber gain during event such as cornering would not exceed and become positive, during which the wheel will lose contact with the surface and there would be more slipping. The camber gain is expected, from this result, to be in limits such that wheel will maintain contact grip with surface during cornering event.

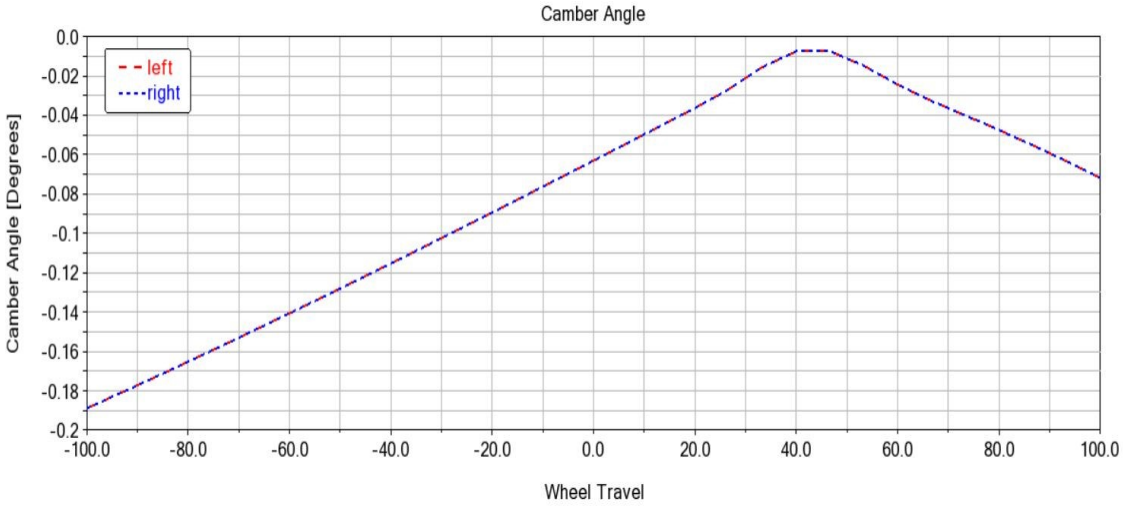

Fig. 3.6. Camber angle variation

4. FSAE VEHICLE MBD MODELS

The vehicle under study is FS car previously built by the IUPUI students involved in the Formula SAE competitions. The vehicle is converted from IC engine to complete electric vehicle. As mentioned earlier, the intentions of this study is to understand its dynamics and handling parameters. The vehicle's full model is assembled from the previous example of McPherson Strut suspension, the vehicle is tested and analyzed. For understanding the complete behavior of a vehicle, individual study of the front and rear suspension is important. Thus, both front and rear suspension are subjected to parallel wheel travel test. The overall vehicle (full body assembled) is subjected to skid-pad test. The details of the model are explained further.

4.1 Model description

4.1.1 Front suspension

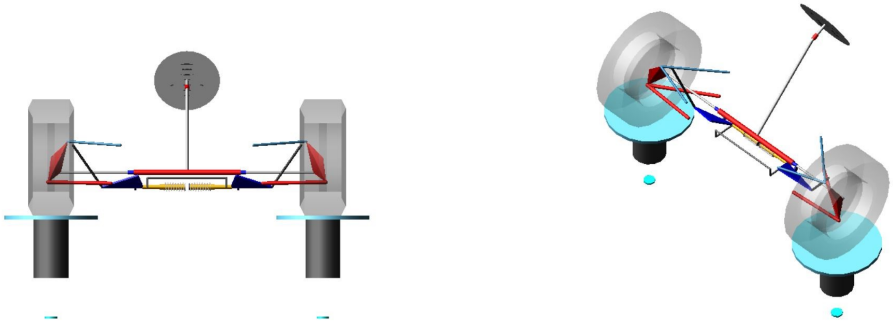

(a) Front view (b) ISO view

Fig. 4.1. Front suspension system for present vehicle

Suspension system are of two types, pushrod type and pullrod type. In pushrod suspension system, a rod is connected in such way that when normal force acts on the tire, the rod transfer the force to the spring-damper system, giving it a pushing motion creating compression in the spring, whereas, a pullrod pulls the spring in the same situation creating expansion of the spring. Note that, since motion in both types are totally opposite, the force acting on the tires completely changes. In this case, the front suspension consists of a pull rod suspension type. Tires are provided with test rig assembly and have a radius of 300mm. Stiffness of tires are by default selected as 200 N/m by default.. For this assembly, CoG selected is 300mm, whereas, for assembly without considering the load of driver, the CoG is 323mm for the assembly. The front suspension under study is assumed to have no parameters such as camber, caster and toe. Length of the upper wishbone is 270.76mm and that of lower wishbone is 323.34mm. No changes have been made to the steering geometry as of now except its offset which is set to 40mm. The spring and damper system are fixed on the bottom of the car 2 inch (50.8mm) from the bottom ground.

4.1.2 Rear suspension

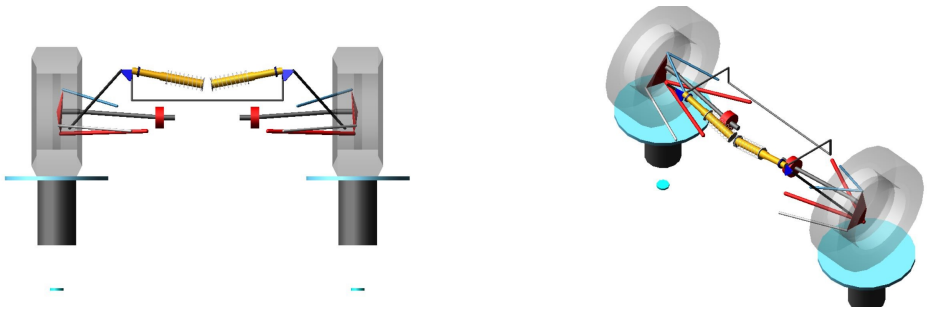

(a) Front view (b) ISO view

Fig. 4.2. Rear suspension system for present vehicle

As opposed to the front suspension, the rear suspension is push-rod suspension type and their opposite behavior can also be seen from the force results which will

be discussed in the later section. The radius of the tire is again kept same for rear suspension as well as that of front suspension. Pushrod is connected to the lower wishbone and connected to the suspension which are mounted above the chassis. Like front suspension, even rear suspension has tie rods. But the major difference that for front suspensions are used for providing steering input or momentum and for rear suspensions, tie rods are used as rigid supports to keep tires from creating unnecessary toe variations. For front wishbone, length is 249.936mm and rear wishbone length is 397.25mm.

4.1.3 Full vehicle assembly

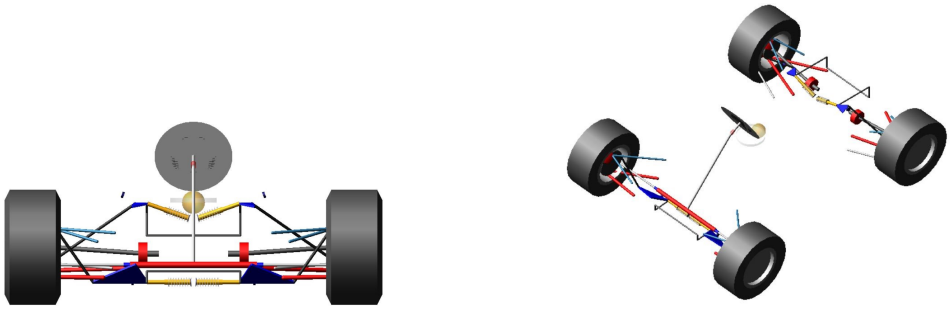

(a) Front view (b) ISO view

Fig. 4.3. Full vehicle assembly for present vehicle

A full body vehicle assembly is possible using both front and rear assemblies. Along with that, powertrain, brake 4W disc and chassis model is also included. Steering system is part of the front assembly and is called upon along with the front suspension assembly. The total wheel base for the vehicle is 1543mm and track is 1423mm. Anti-roll bars both in front and rear suspension are part of their individual assembly and are connected to the outboard point of spring damper system. The chassis width calculated is 497.88mm which is rounded up to 500mm for calculation and inboard pivot point's reasons. Overall weight of the vehicle is 250kg along with driver. Calculations are in reference to [15].

4.2 Vehicle tests

4.2.1 Parallel wheel travel test for front suspension system

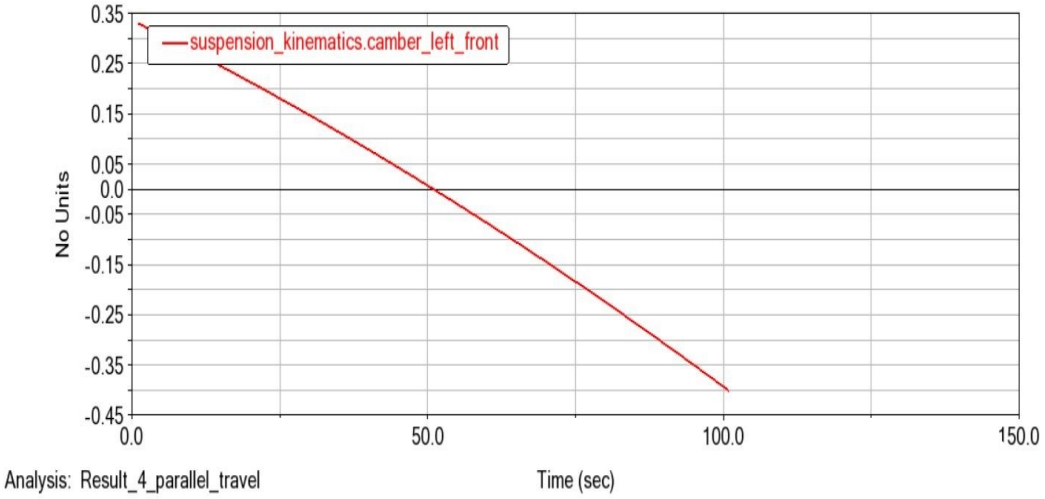

Fig. 4.4. Camber variation for front suspension system

With application of force from test rig in normal direction, the wheel travels from -25mm to 25mm in given time frame of 100 seconds. Note that the results shown are for left tire. Since the test is parallel wheel travel test, the behavior of both tires is the same. Thus, for variation in both tires shows similar behavior and graph for one tire is mentioned in figure 4.4. The camber behavior in the above graph can be seen varying from 0.35 deg which is at the bottom position of the tire during wheel travel test to -0.45 at top most point of the wheel travel and the graph is decreasing linearly. The reason for the camber angle to be positive during the start of the test is that, unlike, McPherson strut example, the restriction in lengths of arm length does not keep the tire from tilting outward. Even though the change in camber is close to 1 deg, wheel tends to get a positive camber during a droop condition and the positive angle is undesirable as it might result in more positive gain during turning on the outer tire which might result in loss of traction.

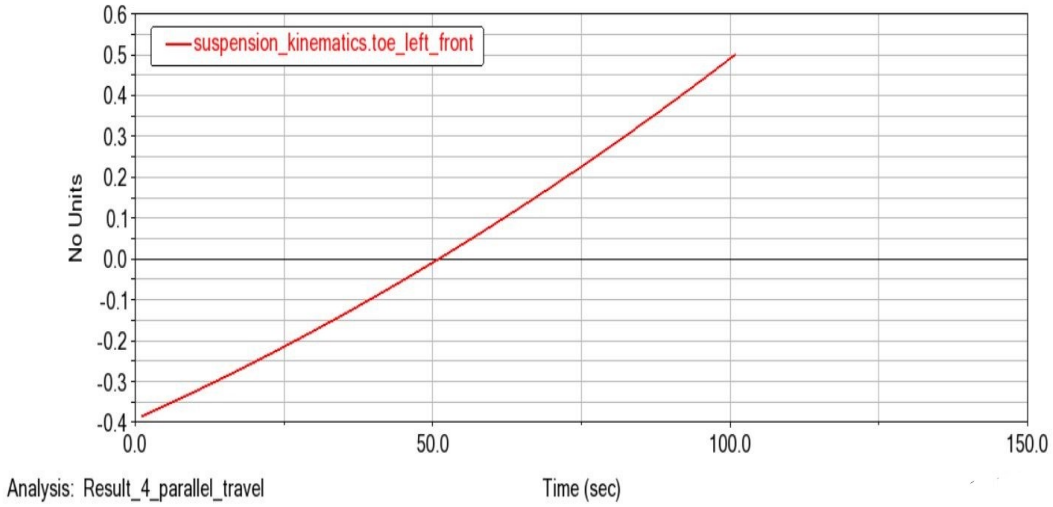

Fig. 4.5. Toe variation for front suspension system

From figure 4.5, we can observe that the toe angle for the vehicle keeps on increasing as the wheel travels upward. The exact same behavior can be observed in Macpherson strut example as well. The only difference is that, in macpherson strut, the displacement of the wheel is from -100 mm to 100 mm and in current model of FSAE the simulation is run for -25 mm to 25 mm. Although the values are different but if the current simulation is run in similar boundary conditions, the graph pattern would be similar for toe angle. During bump, the toe angle becomes positive after 50th second. The change in toe angle is less than 1 deg. But, as mentioned, the toe angle tends to get positive which can lead it to lose traction during a dynamic event and gives the vehicle aerodynamic disadvantage. The force acting on the tire behaves strangely. When at the bottomest position, the spring is compressed as the type of suspension is pullrod suspension and the alignment of the front suspension. Thus the force acting on the outer pushrod joint is negative. The force acting on the tire from the test rig is also considered negative as it is directed downwards. The weight acting on individual tire is considered positive and acts in downward direction. So during the test, overall normal force is a summation of all the forces acting on the tire and turns out to be negative due to the spring force and test rig force directed

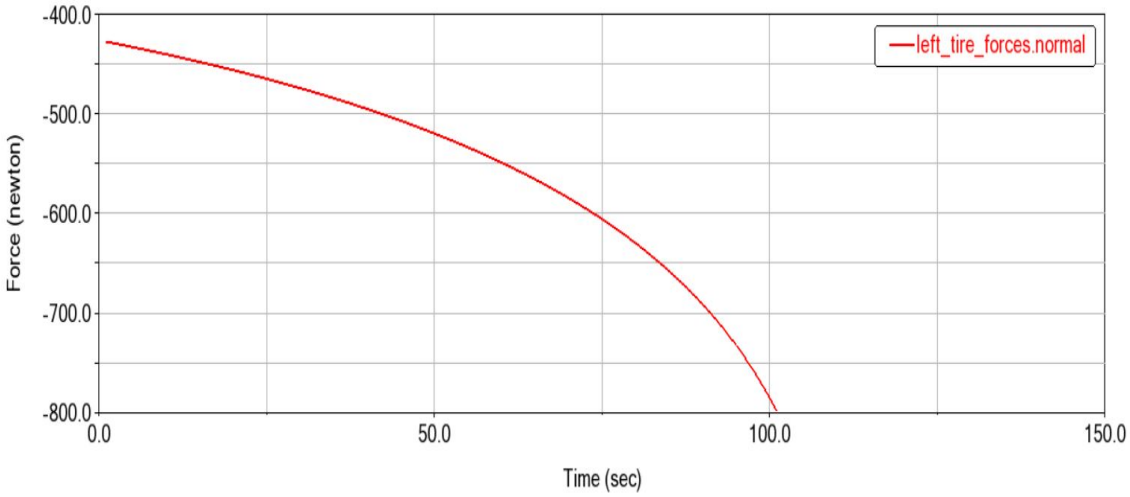

Fig. 4.6. Normal force variation for front suspension system

upwards and the only force acting downwards is positive. As the simulation time increases, the magnitude of force keeps on increasing. As mentioned, the negative value is due to the motion of spring which is completely opposite to that of pushrod, but the magnitude tends to increase with the test rig. For further understanding

Fig. 4.7. Motion ratio for front suspension system

the motion transmission to spring, we need to find the motion ratio of the system,

i.e., ratio of spring travel vs wheel travel. The slope of this graph provides us with motion ratio and since motion ratio does not have a single magnitude, motion ratio for multiple points can be calculated to eventually find frequency and its variation with time. As the tire moves from -25 mm to 25 mm, the spring length goes from 90 to 107 mm which again is due to the pull rod suspension system. It is essential

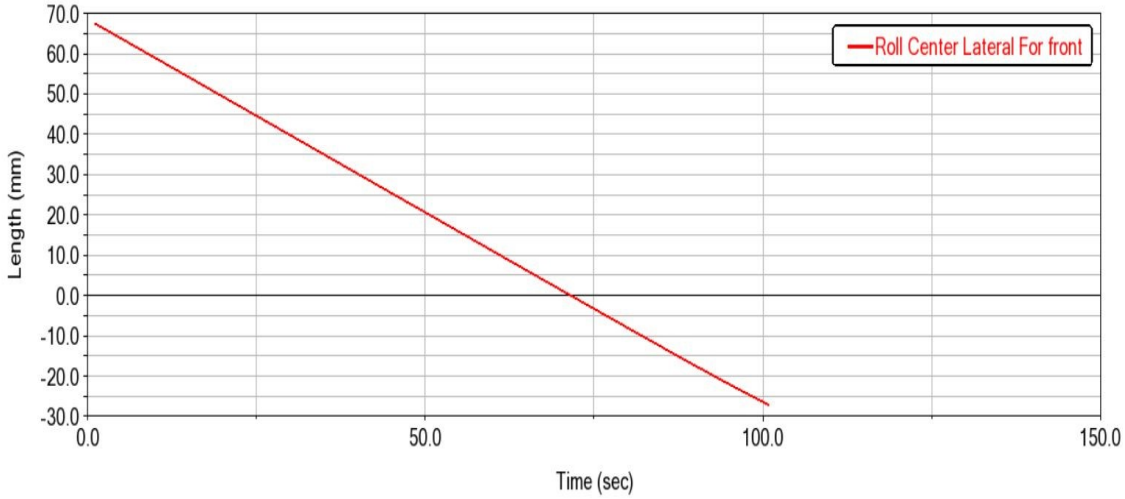

Fig. 4.8. Roll center location for front suspension system

to observe roll center height variation for the front suspension system to study the lateral load transfer in the front suspension system. The range goes from 70 mm at initial stage, i.e., 0 second and linearly goes down till -27 mm approx. The roll center height in some cases is kept down intentionally but has a great influence on lateral load transfer in upcoming section.

4.2.2 Parallel wheel travel test for rear suspension system

Rear suspension system behaves in the exact same manner as front suspension. The could be again due to the same reason and no camber presence. The value of camber variation is different from the front suspension and difference is more than 4 deg in rear suspension system. This makes the rear suspension more unstable

during constant radius turning during which the tire would gain camber more than desired. This can lead the tire to lose contact with the ground, decreasing its friction coefficient, thus, decreasing the lateral frictional force acting on the vehicle essential to keep it in equilibrium.

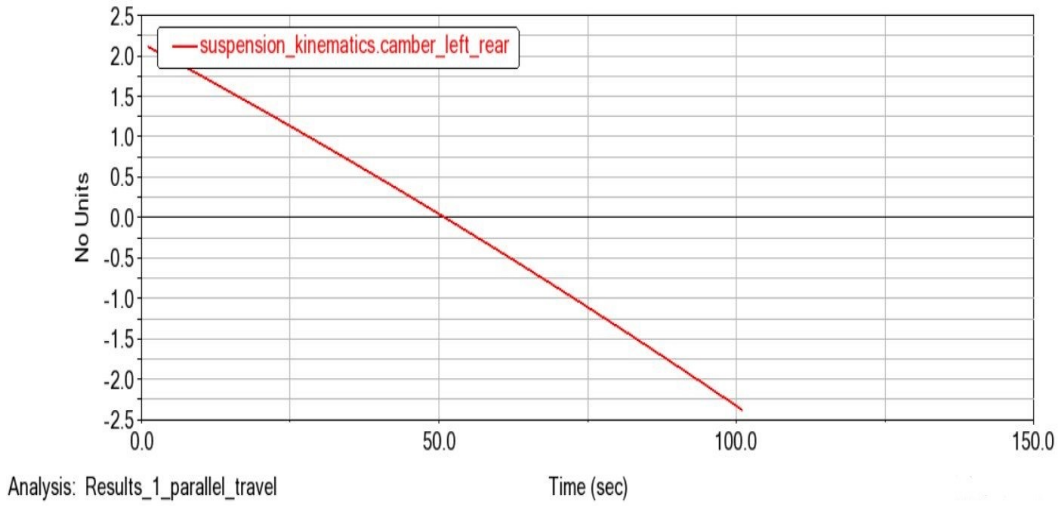

Fig. 4.9. Camber variation for rear suspension system

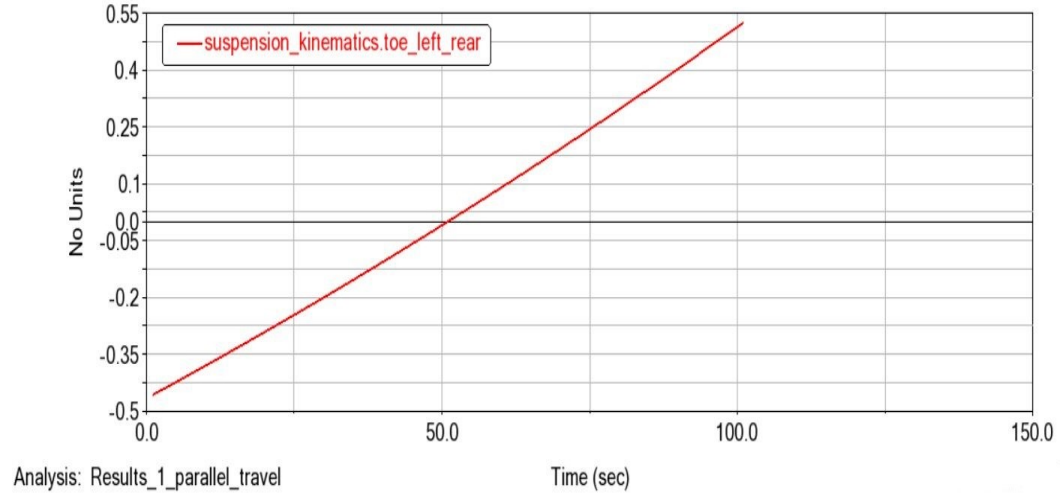

Fig. 4.10. Toe variation for rear suspension system

Comparing figure 4.4 , the toe angle variation in rear suspension system is similar to the toe angle behavior as in front suspension system. During vertical travel, the toe angle is negative, i.e. the tire is pointed inwards towards the centre of chassis at the start of the simulation. This angle changes to zero at the 50th second and keeps on increasing further. At the end of simulation, the tire is pointing outward which again as explained before, gives a disadvantage during events like acceleration by aerodynamic point of view.

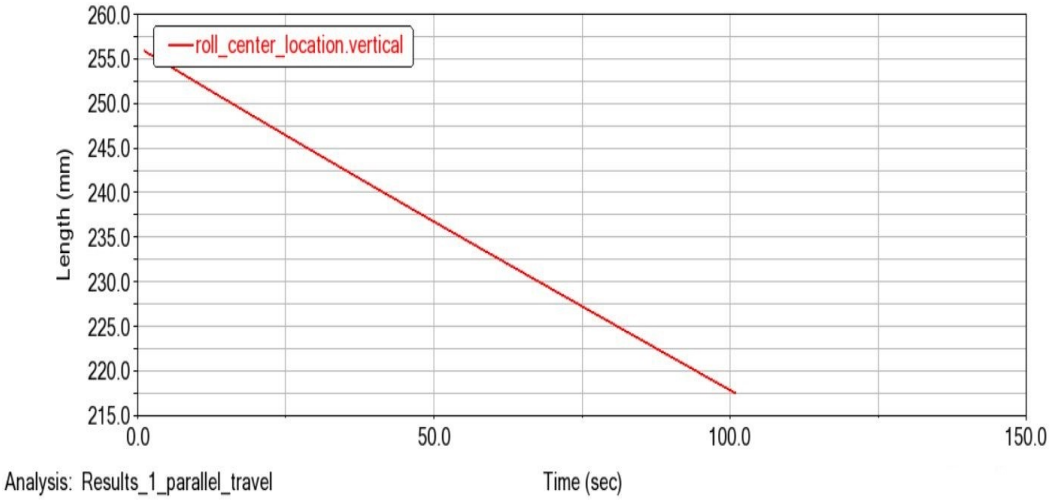

Fig. 4.11. Roll center location for rear suspension system

From figure 2.4, roll center height can be found out by the intersection of the lines of wishbones. Since the simulation starts from the bottom point, the wishbones are pointed upwards. Due to this, the lines are connected above and the height appears at 255 mm approx during start of simulation.The wishbones outer pivots start going up which inclines it as the inboard pivots do not move.

As the rear suspension is pushrod type suspension, the graph has the nature of linearly decreasing till 3 mm of wheel travel from -25 mm. The spring decreases in length till approx 95 mm but disappears after that. After conducting some research, it was found that, at that particular point the spring acts as a rigid link and stops its motion. This is an undesired change as due to this, the force will directly be trans-

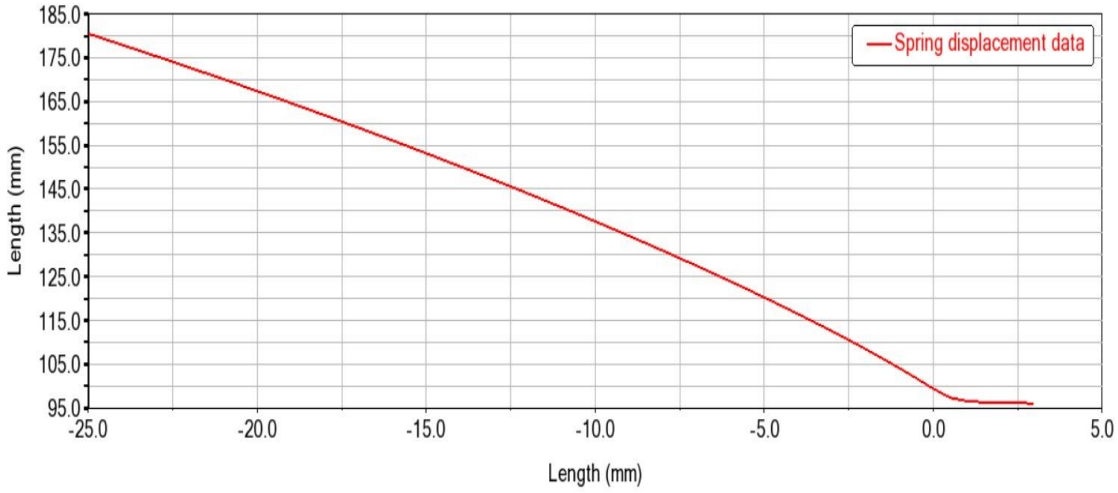

Fig. 4.12. Motion ratio for rear suspension system

mitted to the chassis and in the event of shock, the chassis can sustain damage and along with it the driver. The spring is giving up at almost middle of the experiment and may not be able to complete the test causing failure of the suspension system.

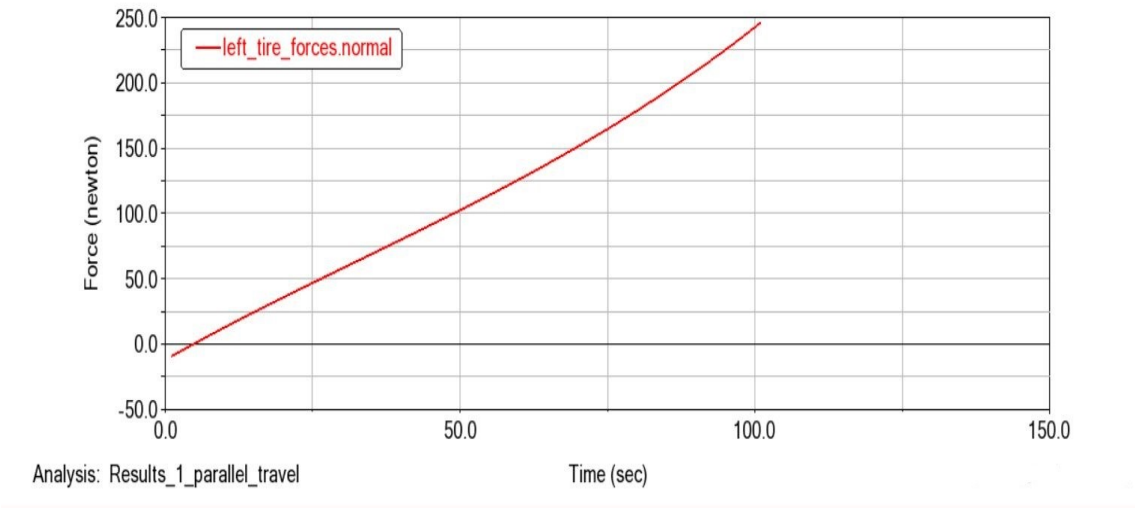

Fig. 4.13. Normal force variation for rear suspension system

The nature of the force graph against time is completely different from the front suspension system. The main reason for this is the type of suspension used. The

suspension type used for the front suspension system is pull rod suspension whereas the rear suspension has push rod type suspension. According to [16], the force acting on both the types of suspension system is opposite to each other. All the while, their magnitude could be in the same range their direction is completely opposite to each other.

4.2.3 Skid-pad test for full vehicle assembly

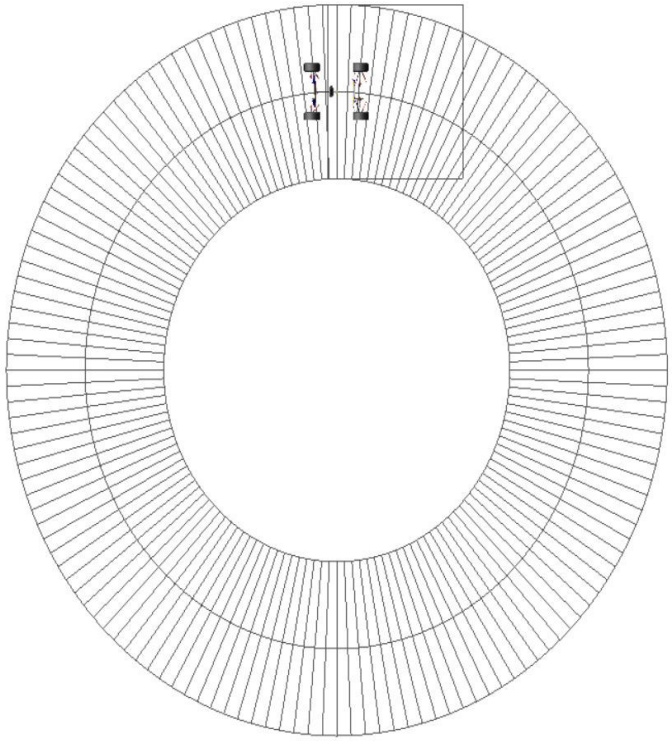

Fig. 4.14. Skid-pad test

The intention of performing skid pad test is to understand maneuverability of the vehicle under test. In the skid pad test, the vehicle (complete assembly) is given a circular path of 8 metre radius (16 metre diameter) to move at a constant velocity. This test is specifically designed to understand vehicle behavior when it is rotating in a circle and with constant velocity and observe forces acting on the vehicle and

how the alignment of the vehicle contributes to the performance of the vehicle in cornering events. In this test, slip angle for the vehicle is studied by performing this test in two conditions, first, by keeping a constant acceleration and second by keeping velocity constant. By performing each test, slip angle behavior in both the front and back suspension system is observed and their respective results are shown below. For constant acceleration type skid pad test, the initial velocity is given as 10 km/hr and final velocity is given as 80 km/hr with 100 steps and steering angle of 30 deg for the entire test. Duration of this test is also set for 10 seconds. In the second test, the velocity is kept constant and of magnitude 20km/hr throughout the test. This test too is run for 10 seconds and constant steer angle of 30 deg. The main determination of slip angle is to find out how it affects latitudinal force acting on the vehicle and what parameters can be considered during design to avoid the unnecessary slip angle

At constant acceleration:

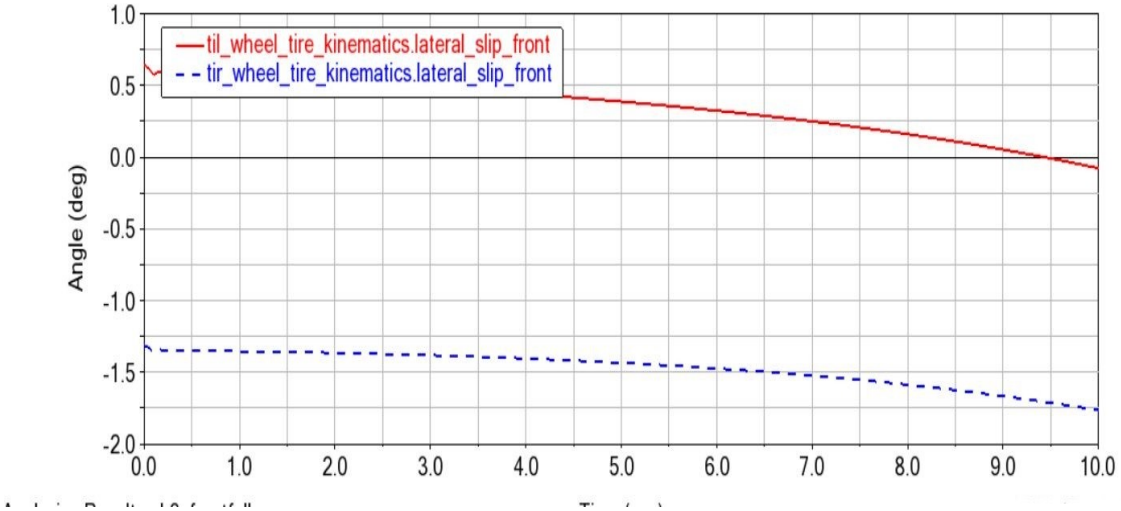

Fig. 4.15. Tire side slip angle in front at constant acceleration

In order to study overall slip angle, it was essential to study tire side slip angle of front and rear tires. MBD model uses the Pajecka Tire model for performing analysis.

In figure 4.15, the variation in tire side slip for both tires is provided by graphical presentation. The intention of providing both left and right tires is to show that the behavior is similar in both tires even though their range is different.

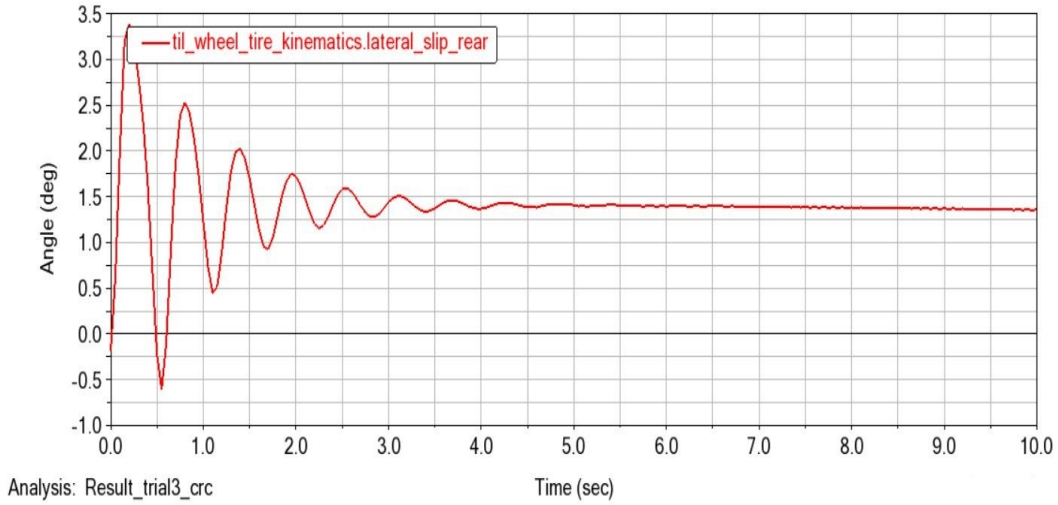

Fig. 4.16. Tire side slip angle in rear at constant acceleration

As it can be seen from figure 4.15, the tire side slip angle reduces constantly over a period of time. This phenomenon is helpful to understand what condition the vehicle is in out of the three steer conditions [17],i.e, Under-steer, over-steer and normal steer. In under-steer, the vehicle tends to go outside the desired path when the front slip angle is more than the rear slip angle. In under-steering, the front tire side slip angle becomes more than rear tire side slip angle, due to which the car tends to go outside the desired path. In over-steering, front tire side slip angle is less than rear tire side slip angle and the vehicle tends to go inside towards the center. In neutral steering, the front tire side slip angle is equal to rear tire side slip angle.

In figure 4.16, tire side slip angle for rear tire oscillates from -0.25 deg to approx 3.4 deg, which is its maximum amplitude and reduces with time, after which it becomes constant at approx 1.4 deg till the end of simulation. Comparing both graphs from figure 24 and 25, the front tire side slip angle is more than the rear tire side slip angle which indicates under-steering.

At constant velocity:

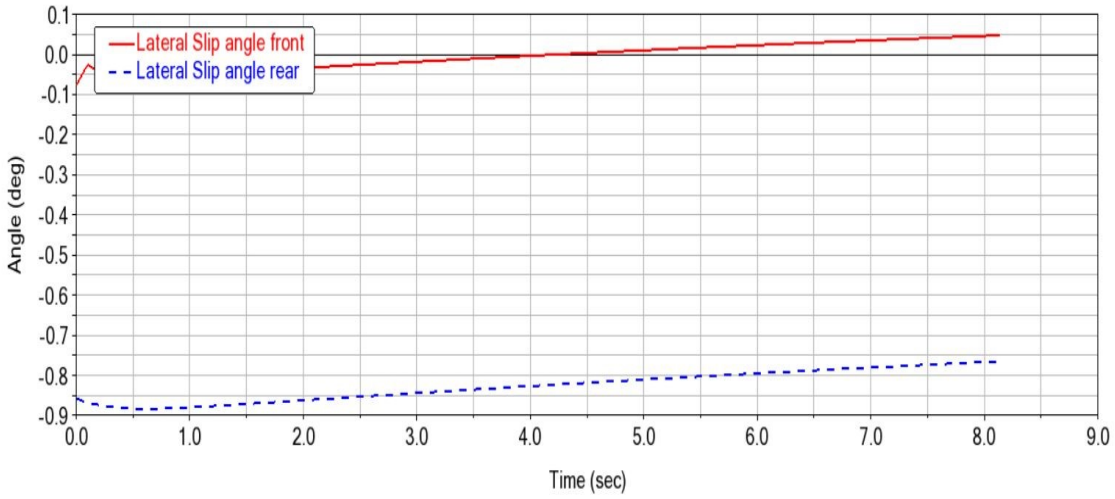

Fig. 4.17. Tire side slip angle in front and rear at constant velocity

At constant speed, the trend shown by the graphs are completely different. From figure 4.17, it can be observed as a gradual increase in front tire side slip angle which has its starting point from approx -0.010 deg and rises up to 0.06 deg which is at 8th second of the test simulation. The graph has positive slope unlike the front tire side slip angle graph with constant acceleration with oscillations are the beginning of the simulation. In comparison with that is the rear tire side slip angle which is lower in value than the front and has value ranging from -0.85 deg to -0.85 within the 8 Tire side slip angle at constant speed does not stabilize like the one with constant acceleration. In Fact it keeps on increasing gradually till 6.5 second of simulation where it stops at approx 0.434 deg. From it can again be observed that the vehicle is under under-steer case as the front tire side slip angle is more than the rear tire side slip angle.

Yaw rate of the vehicle is directly proportional to the both front tire side slip and rear tire side slip angle which can be discussed in equations. Since the yaw rate is

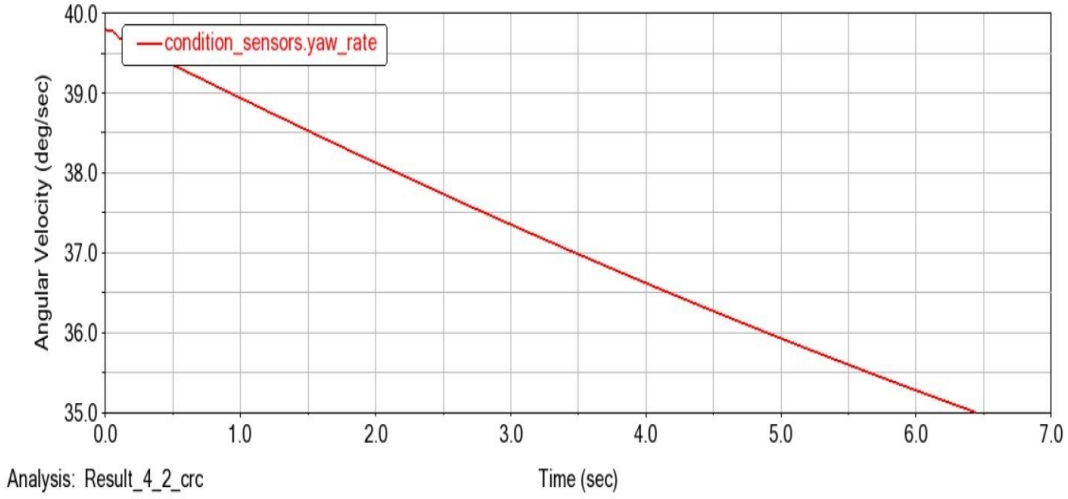

Fig. 4.18. Yaw at constant acceleration

maximum at the beginning of the simulation and gradually reduces to zero over time, thus, the initial turbulence is reduced over time in tire side slip angles.

5. WHEEL MODEL

With reference to [16], equations are used to understand the behavior of tire forces. The ultimate aim of this wheel model is to find frictional forces. For that, initially the equation of dynamic casters are given. For finding dynamic casters, some parameters must be known, velocity of chassis (v_{COG}), yaw rate ($\psi\cdot$), and vehicle side slip angle (α).

$$\eta_L = \frac{1}{2} * (l_0 + l_1 * \frac{F_z}{F_{z^0}}) and \tag{5.1}$$

$$\eta_S = 3 * \eta_L * tan(\alpha) + \frac{F_y}{c_{press}} \tag{5.2}$$

where,

η_L = *Longitudinal dynamic caster*

η_S = *Lateral dynamic caster*

F_{z^0} = *Nominal vertical force*

c_{press} = *parameter to correct tire pressure*

l_0 = *caster parameter*

l_1 = *caster parameter*

Therefore from reference, the distances are given as,

$$r_{FL} = ((l_F - \eta_{LFL} cos(\delta_w) + \eta_{SFL} sin(\delta_w))^2 + (\frac{b_F}{2} - \eta_{SFL} cos(\delta_w) - \eta_{LFL} sin(\delta_w))^2)^{\frac{1}{2}} \tag{5.3}$$

$$r_{FR} = ((l_F - \eta_{LFR} cos(\delta_w) + \eta_{SFR} sin(\delta_w))^2 + (\frac{b_F}{2} + \eta SFR cos(\delta_w) - \eta LFR sin(\delta_w))^2)^{\frac{1}{2}} \tag{5.4}$$

$$r_{RL} = ((l_R + \eta_{LRL})^2 + (\frac{b_R}{2} - \eta_{SRL})^2)^{\frac{1}{2}} \tag{5.5}$$

$$r_{RR} = ((l_R + \eta_{LRR})^2 + (\frac{b_R}{2} - \eta_{SRR})^2)^{\frac{1}{2}} \tag{5.6}$$

where,

r_{FL} = *Distance of front left tire from center*

r_{FR} = *Distance of front right tire from center*

r_{RL} = *Distance of rear left tire from center*

r_{RR} = *Distance of rear right tire from center*

Also, each angle associated with respective distance can be given as,

$$\vartheta_{FL} = arctan[\frac{(b_f/2) - \eta_{SFL}cos(\delta_w) - \eta_{LFL}sin(\delta_w)}{l_F - \eta LFLcos(\delta_w) + \eta_{SFL}sin(\delta_w)}] \tag{5.7}$$

$$\vartheta_{FR} = arctan[\frac{l_F - \eta LFRcos(\delta_w) + \eta_{SFR}sin(\delta_w)}{(b_f/2) + \eta_{SFR}cos(\delta_w) + \eta_{LFR}sin(\delta_w)}] \tag{5.8}$$

$$\vartheta_{RL} = arctan[\frac{l_R + \eta LRL}{(b_R/2) - \eta_{SRL}}] \tag{5.9}$$

$$\vartheta_{RR} = arctan[\frac{(b_R/2) + \eta_{SRR}}{l_R + \eta_{LRR}}] \tag{5.10}$$

5.1 Wheel slip calculations

According to this wheel model in reference with [16], the slip of the wheel can be calculated in two conditions, first braking and second in driving condition, thus respective equations are given below,

For Braking,

$$v_R cos\alpha \leq v_W \tag{5.11}$$

$$s_L = \frac{v_R cos\alpha - v_W}{v_W} \tag{5.12}$$

$$s_S = \frac{v_R sin\alpha}{v_W} \tag{5.13}$$

For Driving,

$$v_R cos\alpha \geq v_W \tag{5.14}$$

$$s_L = \frac{v_R cos\alpha - v_W}{v_R cos\alpha} \tag{5.15}$$

and,

$$s_S = tan\alpha \tag{5.16}$$

Thus, a resultant of above slip can be given as,

$$s_{Res} = \sqrt{s_L^2 + s_R^2} \tag{5.17}$$

where,

v_R = *Desired direction of the vehicle*

v_W = *actual direction the vehicle moves*

5.2 Tire side slip angle

The tire side slip angle can be calculated using two methods,

1. Four Wheel Method or Wheel Velocity Vector Method
2. Single track or Bicycle Model Method

5.2.1 Four wheel method

In this method, once the direction of the wheel is known, the calculation of Slip angle can be done geometrically. As defined before, the tire slip angle is the angle between the desired direction of the wheel and the direction in which it is actually moving. For calculation, the slip angles can be calculated using below equations [16]:

Using Four Wheel Method,

$$\alpha_{FL} = \delta_w - arctan[\frac{v_{COG} * \beta + \psi \cdot r_{FL} * cos\vartheta_{FL}}{v_{COG} * \beta - \psi \cdot r_{FL} * sin\vartheta_{FL}}] \tag{5.18}$$

$$\alpha_{FR} = \delta_w - arctan[\frac{v_{COG} * \beta + \psi \cdot r_{FR} * sin\vartheta_{FR}}{v_{COG} * \beta + \psi \cdot r_{FR} * cos\vartheta_{FR}}] \tag{5.19}$$

$$\alpha_{RL} = -arctan[\frac{v_{COG} * \beta - \psi \cdot r_{RL} * sin\vartheta_{RL}}{v_{COG} - \psi \cdot r_{RL} sin\vartheta_{RL}}] \tag{5.20}$$

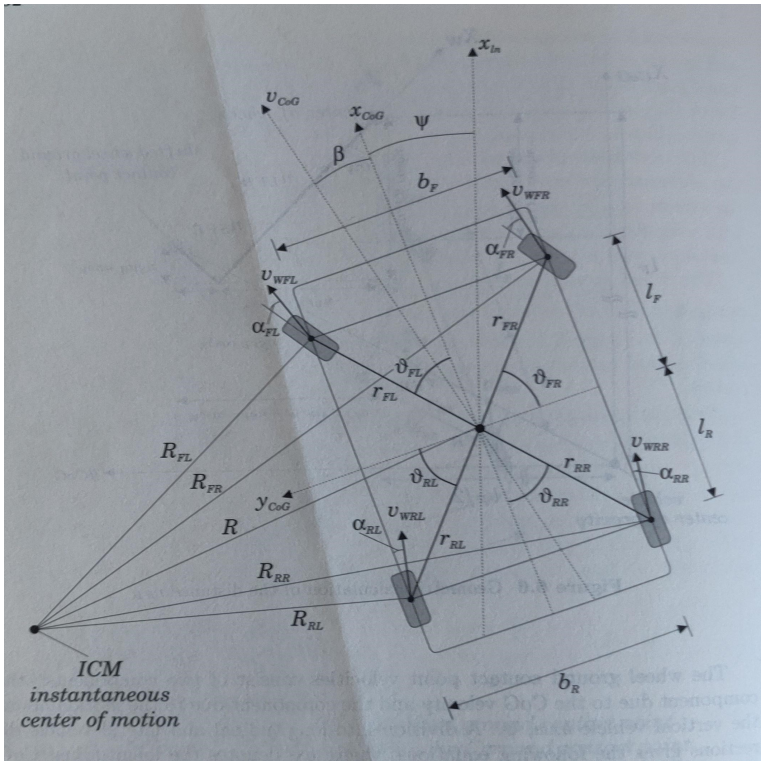

Fig. 5.1. Four wheel method [16]

$$\alpha_{RR} = -arctan[\frac{v_{COG} * \beta - \psi \cdot r_{RR} * cos\vartheta_{RR}}{v_{COG} - \psi \cdot r_{RR} sin\vartheta_{RR}}] \tag{5.21}$$

where,

α_{FL}= *Slip angle for front left wheel*

α_{FR}= *Slip angle for front right wheel*

α_{RL}= *Slip angle for rear left wheel*

α_{RR}= *Slip angle for Rear right wheel*

5.2.2 Single track or bicycle model method

In a single track method [18], the wheels on the same axis are considered to be one unit. Thus in this method a single side slip angle is calculated for both left and right wheel. In this method, an instantaneous centre is considered which when connected to the CoG of the vehicle is perpendicular. Front slip angle and rear slip angle can

be calculated using this method if the body slip angle of the vehicle is known. The below figure explains the direction of the velocity vector for front and rear wheels. Thus the equations for front and rear slip angle is given as:

$$\alpha_F = -\beta + \delta_w - (\frac{l_F * \dot{\psi}}{v_{COG}}) \tag{5.22}$$

and,

$$\alpha_R = -\beta + (\frac{l_R * \dot{\psi}}{v_{COG}} \tag{5.23}$$

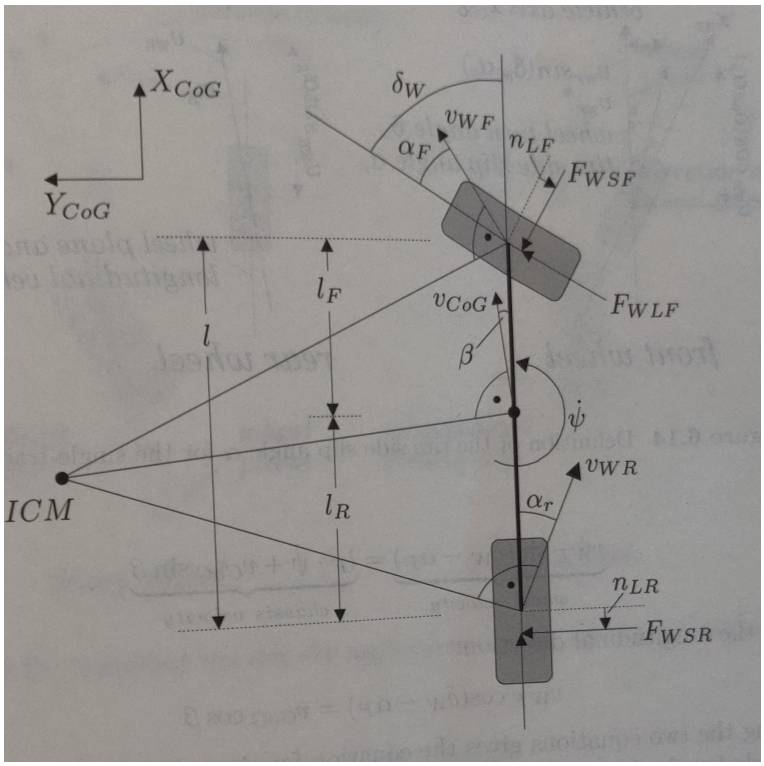

Fig. 5.2. Single track model [16]

In Figure 4.16 oscillations can be observed during the initial phase which tends to disappear as time proceeds. It can be observed from the above equation, the tire side slip angle is proportional to the yaw rate of the vehicle. From Figure 4.18, it can be observed that the yaw rate decreases with time and comes to a halt after 6.3 seconds approximate. From this equation, the behavior of the tire and yaw rate can be linked

and considered responsible for oscillations during the initial phase. Currently, due to its accuracy and low computational cost, most works and software use bicycle models for calculation [16]

5.3 Friction coefficient

In any tire model, the derivation of slip angle is associated with formulation of longitudinal and latitudinal force. In this particular wheel model, frictional force in both longitudinal and lateral direction is derived. For calculation of frictional force, determination of friction coefficient is essential. Therefore, the longitudinal and lateral coefficient can be given as,

$$\mu_L = \mu_{Res} * \frac{s_L}{s_{Res}} \tag{5.24}$$

$$\mu_S = \mu Res * \frac{s_S}{s_{Res}} \tag{5.25}$$

where,

μ_L = *Longitudinal Co-efficient of friction*

μ_S = *Lateral Co-efficient of friction*

μ_{Res} = *Resultant Co-efficient of friction*

s_L = *Longitudinal slip*

s_S = *Lateral slip*

s_{Res} = *Resultant slip*

6. SUSPENSION MODEL

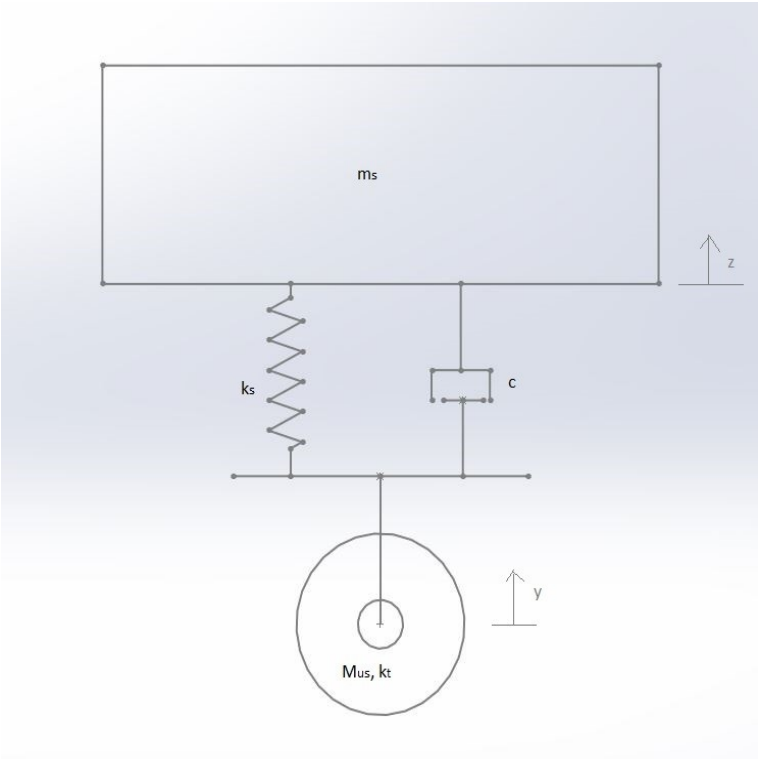

Fig. 6.1. Suspension model

In order to study the vertical motion of the vehicle, it is essential to break down the vehicle in four parts. Each part of the vehicle is divided in such a way that it contains suspension system for a single tire and is also known as Quarter car model. A simple representation of suspension system is shown using block diagram in figure 6.1. The mass of the vehicle is considered as sprung mass and is denoted as m_S. Mass of components and systems whose weight is supported by the suspension system is considered as the sprung mass of the vehicle. Note that the mass of the vehicle overall is divided in 4 equal parts due to the quarter car model. Thus the mass m_S is 1/4th

of the total sprung mass of the vehicle. The mass of the vehicle that is not supported by the suspension system is considered in the unsprung mass category (m_{US}). Tires and wishbones consist of the majority of the unsprung mass category. The suspension model in figure 31 can be broken down as, the sprung mass (m_S) is being supported by spring-damper system with k_S being the stiffness of the spring and c is the damping coefficient. and $m_{US}$is the unsprung mass of the vehicle which is the mass of the tire and k_t is stiffness of the tire. The force acting on the system can be given in the following equations. y and z is the displacement of the system as shown in the figure 6.1.

The equations of motion can be given as follows:
for sprung mass,

$$m_S z^{\cdot\cdot} = -c(y^{\cdot} - z^{\cdot}) - K_S(z - y) \tag{6.1}$$

for unsprung mass,

$$m_{US} y^{\cdot\cdot} = -c(y^{\cdot} - z^{\cdot}) - K_{US}(z - y) - K_T(y - r) \tag{6.2}$$

where,
r = *road profile input*

6.1 Suspension motion ratio

The suspension of the vehicle functions not only to absorb shocks from the road and abnormalities on it but also to maintain contact of the tire with the ground. It has to ensure that regardless of the angles the tire or system has, the tire should have optimum contact with the ground even if the tire is changing its position. This can be achieved by transmitting the forces produced and experienced by the tire through to the chassis by use of springs and controlling its rate by use of dampers. The spring in

a car's suspension experiences force and motion based on the motion ratio designed for the system [19]. The motion ratio can be given as follows [20];

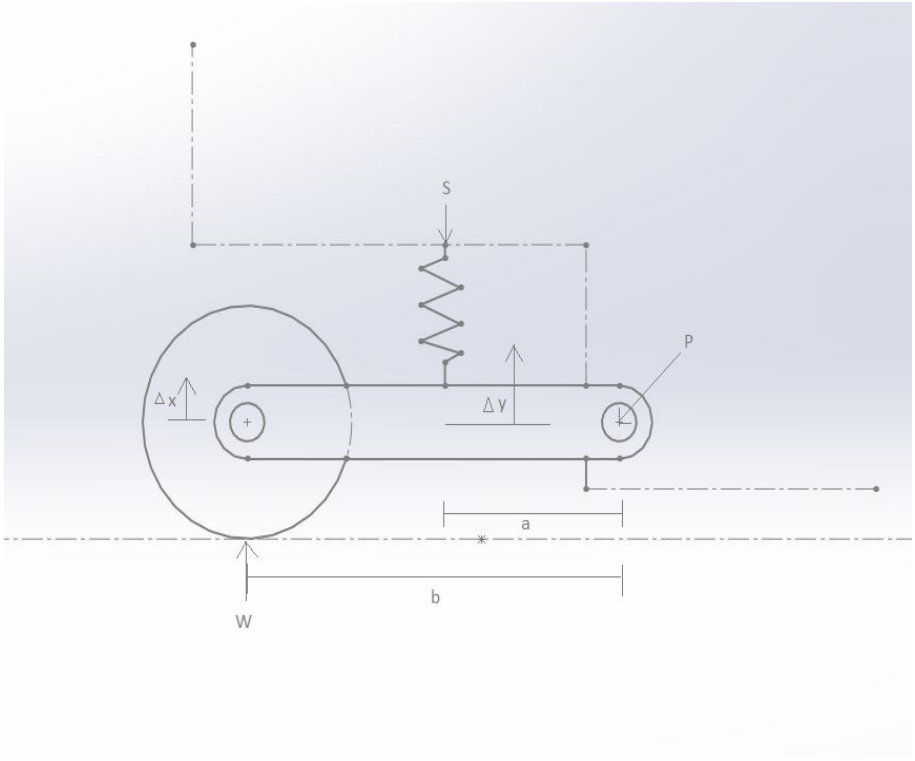

Fig. 6.2. Motion ratio [20]

The displacement ratio is given as,

$$\frac{\Delta x}{b} = \frac{\Delta y}{a} \tag{6.3}$$

therefore,

$$\Delta x = \frac{b}{a} * \Delta y \tag{6.4}$$

where,

$\frac{b}{a}$ = *Mechanical Advantage*

The ratio b/a is considered as a mechanical advantage as it proves to be an amplifying factor for the vertical motion which works in favor of the system [20]. To find the motion ratio in terms of force, summation of moment on a pivot can be used. In a closed system, summation of moments on a pivot is zero. Thus,

$$\Sigma M_P = 0 \tag{6.5}$$

therefore,

$$F_W * b = F_S * a \tag{6.6}$$

thus,

$$F_W = \frac{a}{b} F_S \tag{6.7}$$

where,

$\frac{a}{b}$ = *Motion Ratio*

Since, $b > a$, the force on wheel and spring can said to be $F_W < F_S$,

This equation can also be written in terms of stiffness. For that we need to divide above two equations.

So by dividing equation (6.7) by (6.4), we get,

$$\frac{F_W}{\Delta x} = \frac{F_S}{\Delta y} * (\frac{a}{b})^2 \tag{6.8}$$

therefore, we get,

$$K_W = K_S * (MR)^2 \tag{6.9}$$

where,

K_W = *Tire stiffness*

K_S = *Spring Stiffness*

$\frac{a}{b}$ = *MR = Motion Ratio*

The motion ratio is important to design the desired amount of spring travel for the specific amount of wheel travel. The motion ratio thus can be designed to absorb maximum momentum gained by the suspension when maximum wheel displacement takes place. Thus the effectiveness and performance of the suspension system can be maximized.

6.2 Lateral load transfer

During cornering, it is important to study the lateral load on the wheels to analyze the total load transfer so that the behavior of the tire can be predicted along with its consistency to be in contact with the road. In other words, it is essential to design the suspension system so that it can be used to its maximum efficiency. The system shown in figure 6.3 is a simplified version to study the forces acting on the vehicle. Thus, according to [20] the equation of the lateral load transfer is given as,

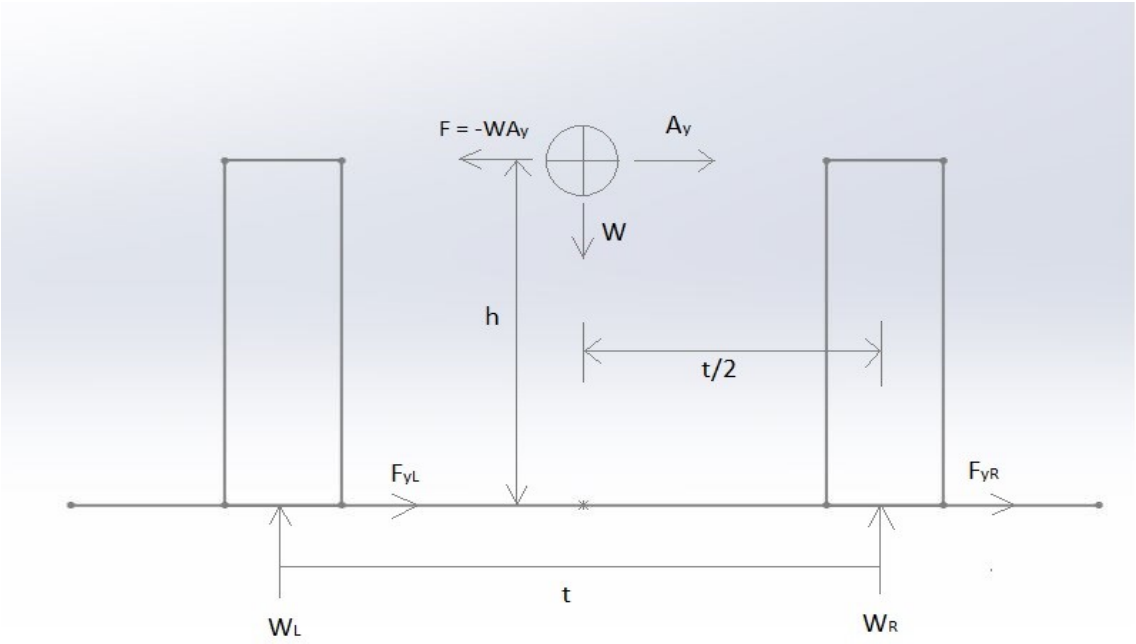

Fig. 6.3. Lateral load transfer [20]

Since the moment across CG is zero, i.e.,

$$\Sigma M_{CG} = 0 \tag{6.10}$$

Therefore, weight transfer is given as,

$$W_L = \frac{W}{2} + W * A_y * \frac{h}{t} \tag{6.11}$$

where,

$\frac{W}{2} \Rightarrow$ *Static Load* and,

$W*A_y*\frac{h}{t} \Rightarrow$ *Lateral Load Transfer*

Although by the above equation we get total load transfer, manipulating the load transfer is difficult. To change or manipulate the total load transfer, the CoG height and track needs to be changed which makes the process complicated and makes it difficult to achieve the desired goal of load transfer. Thus, for design purposes, another approach is considered. Thus, with reference to [20], instead of using total load transfer, the focus is more targeted on three different components,

1. Load transfer from unsprung mass
2. Load transfer from direct lateral force
3. Load transfer from roll

6.2.1 Load transfer from unsprung mass

Unsprung mass mostly consists of tire mass. To change the load transfer from unsprung mass, the mass of tire needs to be changed which changes the characteristics of the tire completely. Due to model limitation, achieving that change is not possible. Thus, the other two components will be taken into consideration.

6.2.2 Load transfer from direct lateral force

According to [20], the load transfer from direct lateral force is responsible for overturning or non-rolling moment. A non-rolling moment means that the moment that does not contribute to the rolling of the vehicle. During an event of cornering,

the lateral force acts on the CG of the vehicle. Thus, this force can be translated to roll center by adding a moment also across the roll center and the moment across roll center can be given as [20],

$$M_\phi = F_y * h_{arm} \tag{6.12}$$

where,

h_{arm} = *Distance between Roll center height and COG height*

The actual lateral transfer due to lateral load can be given as,

$$\Delta W_{RC} = \frac{W_S * A_y * Z_{RC}}{t} * \frac{l - x}{l} \tag{6.13}$$

where

W_S = *Sprung Weight*

Z_{RC} = *Roll center height*

A_y = *Centripetal acceleration*

x = *distance between CG and axle opposite to that being analyzed*

The change in roll center height can be achieved by changing the geometry of the wishbones. Thus, the load transfer from lateral load can be controlled by controlling the roll center height (Z_{RC}). According to [20], this load transfer is not responsible for rolling of the vehicle. Thus, it can be noted that by increasing the roll center height, the moment acting on it might increase but will not result in rolling of the vehicle.

6.2.3 Load transfer from body roll

During cornering, the due to load transfer deflection in the spring on the outer side of the vehicle undergoes and the spring in the inner side of the vehicle tends to go under expansion. This is the result of inertia and thus there is an angular displacement along the roll axis of the vehicle. That displacement is known as roll.

During this condition, the CG also shifts outwards, giving rise to moment. Thus, that moment can be given as,

$$M_\phi = (W_S * A_y * h_{arm} * cos\phi) + (W_S * h_{arm} * sin\phi) \tag{6.14}$$

where,

ϕ = *Roll angle*

$A_y = \frac{v^2}{R*g}$ = *Centripetal Acceleration in terms of g*

h_{arm} = *Distance between RCH and COG*

The body roll is opposed by the roll stiffness provided by the suspension system. This roll stiffness can be given as,

$$k_\phi = k_{\phi f} + k_{\phi r} \tag{6.15}$$

Thus, the stiffness moment opposing the roll can be given as,

$$M_\phi = k_\phi * \phi \tag{6.16}$$

Therefore by comparing above two equations,

$$k_\phi * \phi = (W_S * A_y * h_{arm} * cos\phi) + (W_S * h_{arm} * sin\phi) \tag{6.17}$$

As the roll angle is much smaller,

$cos\phi = 1$ and $sin\phi = \phi$ thus,

$$k_\phi * \phi = (W_S * A_y * h_{arm}) + (W_S * h_{arm} * \phi) \tag{6.18}$$

Therefore,

$$\frac{\phi}{A_y} = \frac{W_S * h_{arm}}{k_{\phi f} + k_{\phi r} - W_S * h_{arm}} \tag{6.19}$$

where,

$\frac{\phi}{A_y}$ = *Roll gradient*

Now that all three component are defined, the total lateral load transfer can be given as [14],

$$\frac{\Delta W}{A_y} = \frac{W_{ua} * Z_{us}}{t_a} + \frac{W_S * Z_{RC}}{t_a} * \frac{l - x}{l} + \frac{k_{\phi a} * W_S * h_{arm} * A_y}{t_a(k_{\phi f} + k_{\phi r} - W_S * h_{arm})} \tag{6.20}$$

where,

$\frac{W_{ua} * Z_{us}}{t_a}$ = *load transfer due to unsprung mass*

$\frac{W_S * Z_{RC}}{t_a} * \frac{l-x}{l}$ = *load transfer due to lateral force*

$\frac{k_{\phi a} * W_S * h_{arm} * A_y}{t_a(k_{\phi f} + k_{\phi r} - W_S * h_{arm}}$ = *load transfer due to body roll*

7. MODIFIED VERSION OF THE FSAE VEHICLE

There were some limitations observed in the current version of the vehicle. Thus, changes were made to the model to improve its performance by keeping the cost minimum. With intention to keep the cost minimum, the changes were limited to only changing the geometry without making major changes to actual parts. The changes and their effects will be briefly explained in the upcoming sections. The modified model is also subjected to the same test conditions in order to compare the changes. Like before, the individual system will be analyzed and then the all systems put together as a full vehicle. Individual suspension system is subjected to parallel wheel travel and the assembly is subjected to skid-pad test (constant radius turning). Next sections explain the individual model and its test results will be explained in the section after that.

7.1 Model description

7.1.1 Front suspension system

To start with front suspension, firstly, the suspension type was changed from pull rod suspension to pushrod suspension. This was done for two reasons, first, the spring and damper system were placed at the bottom of the car at approximately 2 inches from ground (50.8 mm). This means when the diameter of the spring is considered, the distance between the spring and ground is close to 1 inch (25.4mm). Due to this, during the event of bump the spring is bound to make contact with the ground which is in direct violation of the rule that states no part of the vehicle, except the tires, should make contact with the ground and can lead to disqualification. Secondly, the position of the spring matters for appropriate motion ratio. The position of spring

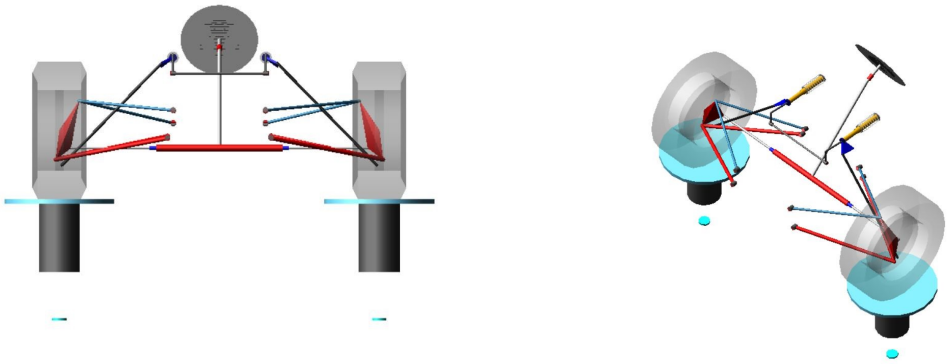

(a) Front view (b) ISO view

Fig. 7.1. Modified front suspension system

and damper can be better explained in comparison and will be explained in brief in the upcoming section. The tire model used is default in the assembly and no changes yet made to the steering system. This model was tested for different camber angles and - 2 deg was decided for the front system.

7.1.2 Rear suspension system

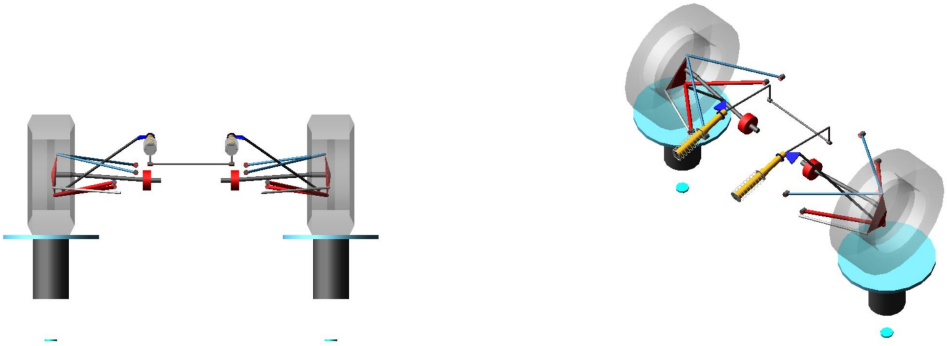

(a) Front view (b) ISO view

Fig. 7.2. Modified rear suspension system

The reason for changing the position is again the motion ratio. The roll center is kept low intentionally as to make the rear suspension system less stiff than the front suspension system. With the intention of making the vehicle oversteer from its current condition, it was essential to make the front suspension system more stiffer than the rear suspension system for the vehicle to overturn. Camber angle comparison is also mentioned in the upcoming figure and from that comparison, the camber angle selected for rear suspension system is -1 deg with the intention of gaining positive camber during extreme conditions. The powertrain as similar to the previous model is given to the rear suspension system. Tire and test conditions are kept constant for comparison purposes. Rear suspension system has similar tie rods which are used as restrictors for the tires. Their length can be adjusted to set a default toe but is kept zero for now and the test is focused on camber angle change only.

7.1.3 Full vehicle assembly

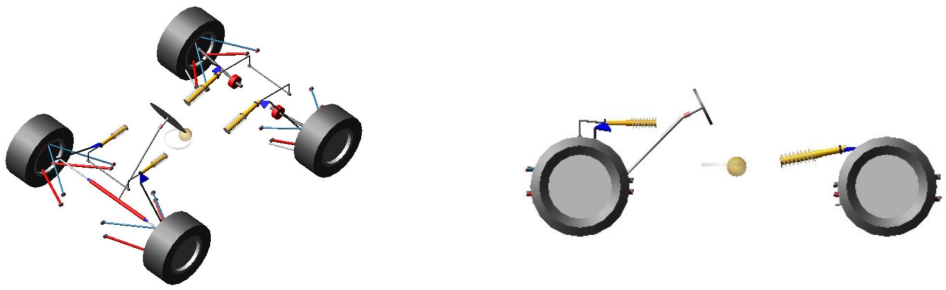

(a) ISO view (b) Side view

Fig. 7.3. Modified full vehicle assembly

The vehicle assembly can be created by calling the front modified assembly and rear assembly together with all other subsystems. Note that, in this experiment, the intention is to make the front suspension system more stiff than the rear suspension system. This will cause the rear to roll more than the front and the vehicle will turn

inward during the constant radius turning test. The front roll center is kept at 80% of the COG and rear at 70% of the CG height. By keeping the height of roll center close to CG decreases the h_{arm} distance. Thus, this decreases the load transfer on front making it more stiff. The main intention in doing so is change the original path of the vehicle and make it more inwards than before. The track of the vehicle is 1432 mm for both front and rear. The wheelbase is 1532 mm. There is a slight increase in wishbone lengths to get a smaller ratio than before. The equations mentioned above are followed for calculations and the results follow trends in accordance with the equation. The graphical trends and explanation will be much more understanding in the test and results section.

7.2 Modified vehicle tests

7.2.1 Parallel wheel travel test for front suspension system

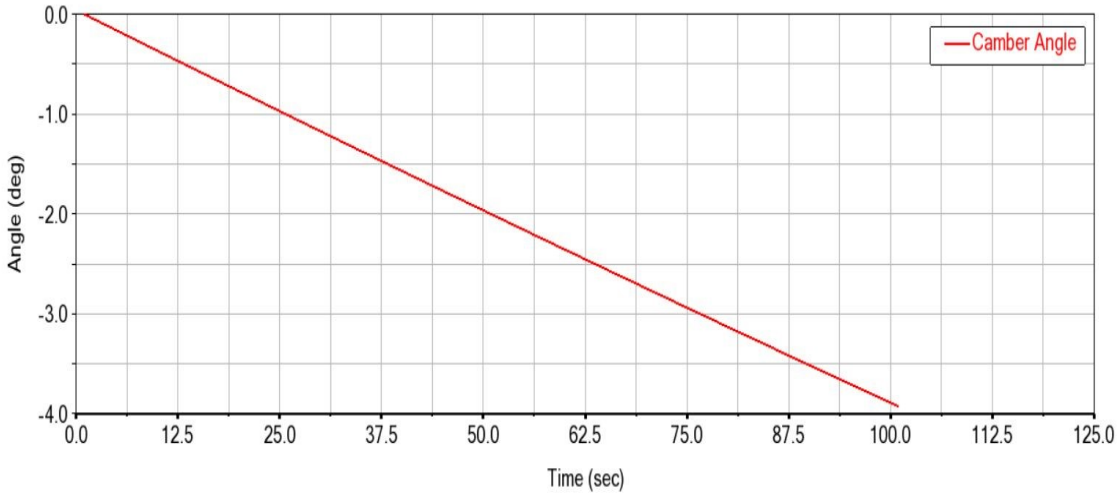

Fig. 7.4. Camber variation for modified front suspension system

As mentioned above the test parameters are maintained same for comparison purpose. The normal force is applied from the test rig on the tires to move the tires from -25 mm to 25 mm as before to study the characteristics after modification. The

time is divided intentionally into more segments for accuracy and the camber angle offset is set of -2 deg. The gradual trend in slope is similar to the previous camber change observed in figure 4.4. Although the values have been changed due to the change in default offset. The negative camber during bump can be seen to reach approximately to -4 deg and the positive camber can as much as 0 deg. The reason behind selecting this camber can be seen in the comparison graph in figure 7.5.

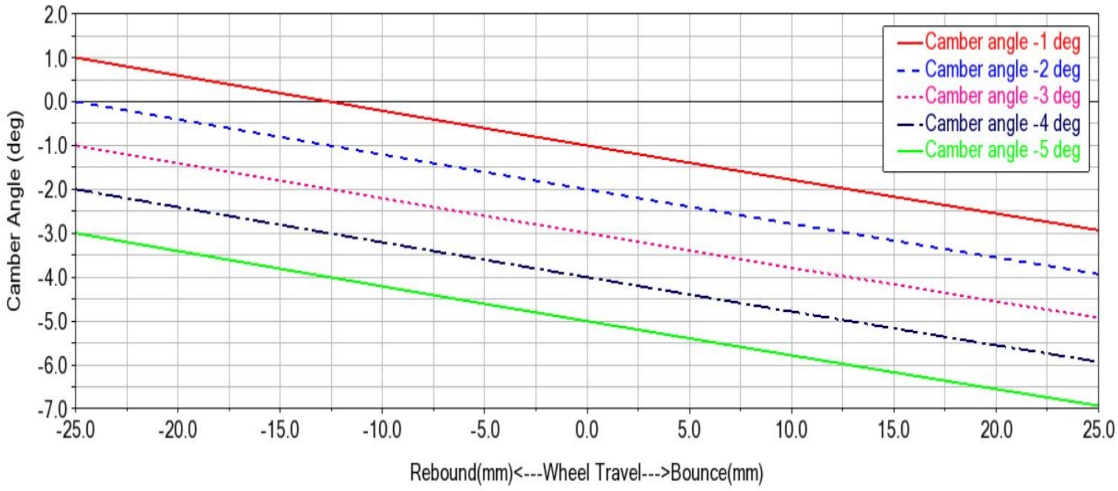

Fig. 7.5. Camber comparison for modified front suspension system

Figure 7.5 is the result of conducting parallel wheel travel test with varying camber angle. The range for test goes from -1 deg to -5 deg. From this comparison, -2 deg offset was selected for the design under study. The reason for selecting -2 deg is that, with -2 deg camber, the wheel in its maximum rebound that is -25 mm, goes till 0 deg camber. This means that, in the event where the wheel gains extreme camber the negative camber offset is nullified and the wheel becomes upright with respect to the ground. This helps in the situation where the vehicle is undergoing corner. During cornering, the wheel in the outermost side tries to incline outwards. By adding negative camber offset of 2 deg, the wheel in that particular condition would be perpendicular to the ground thus gaining maximum contact with the ground and increasing its grip. The reason for not selecting any other camber more than 2 deg is

that during the extreme camber gain, the offset can be nullified to a certain limit and still the wheel will be in negative camber. Even though the angle is not big and the tire maintains its contact with the ground, it is not as good as the 0 deg as in 0 deg the tire is perpendicular thus maintaining the maximum contact possible. Also, by always being in negative camber, the tire starts to wear on the inner side and requires repair or replacement more quickly than anticipated. The reason for not selecting the camber below 2 deg is that, it can be observed that the camber becomes positive and go till 1 deg. This means, in cornering, the tire can gain positive camber till 1 deg and loose contact with the ground which can lead to increase in slip of the vehicle.

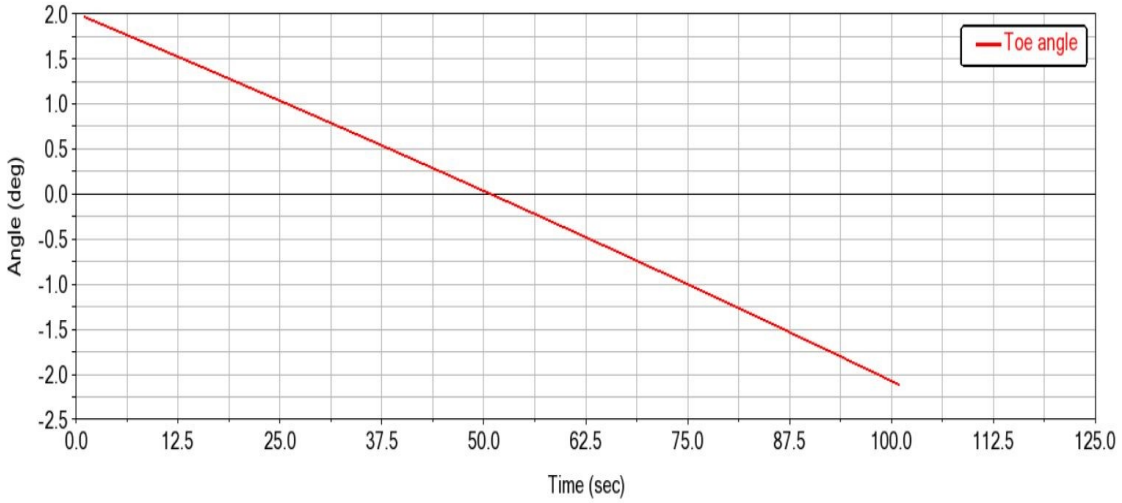

Fig. 7.6. Toe variation for modified front suspension system

By comparing figure 7.6 and 4.5 for toe angle variation, it can be observed that the nature of the graph changes completely. The gradual linerity observed in figure 15 which goes from -0.4 deg to 0.5 deg is now changed to go from 2 deg to -2.2 deg approx. Although the range is short for the previous model, it has to be considered that toe angle was kept neutral for this test and can be modified in future experiments for steering analysis to get desired range and value.

As shown in figure 7.7, the normal force acting on the wheel shows a gradual linear trend with maximum value to be approx 1225 N. The simulation runs for 101 seconds

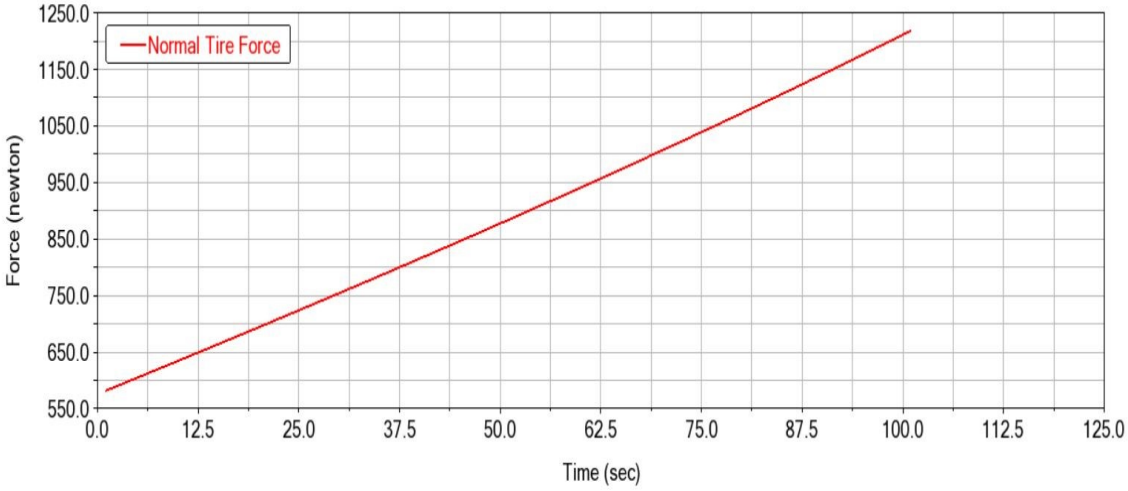

Fig. 7.7. Normal force variation for modified front suspension system

as the initial time was set to 100 seconds. As mentioned before, the trend of graph is greatly manipulated by the type of suspension and spring displacement. When compared with figure 16, the graph clearly shows the opposite trend. As the previous front suspension model was pull rod and the current suspension model under study is pushrod suspension type, the graph nature is completely different. The graph is also influenced by motion ratio of the suspension system and would be discussed further by comparison.

By comparing the motion ratio, we can see that the motion ratio also has opposite sign convention due to the type of suspension system in front. But when considered slop, the previous model has a slope of 1.33 whereas the current modified model has a slope of -0.53. The slope usually means that the motion transmitted from the wheel is slope times the motion in the spring system. With the slope which is more than 1, the graph in figure 16 shows a parabolic like curve. With a slope less than 1 and push rod suspension, the force curve shows gradually increasing linear curve.

Roll center height decreases with increase in time. It can be observed that, even though the roll center height is designed to be 70% of the CG height as shown in figure 7.9., the roll center height neutral position comes out to be a slight more than

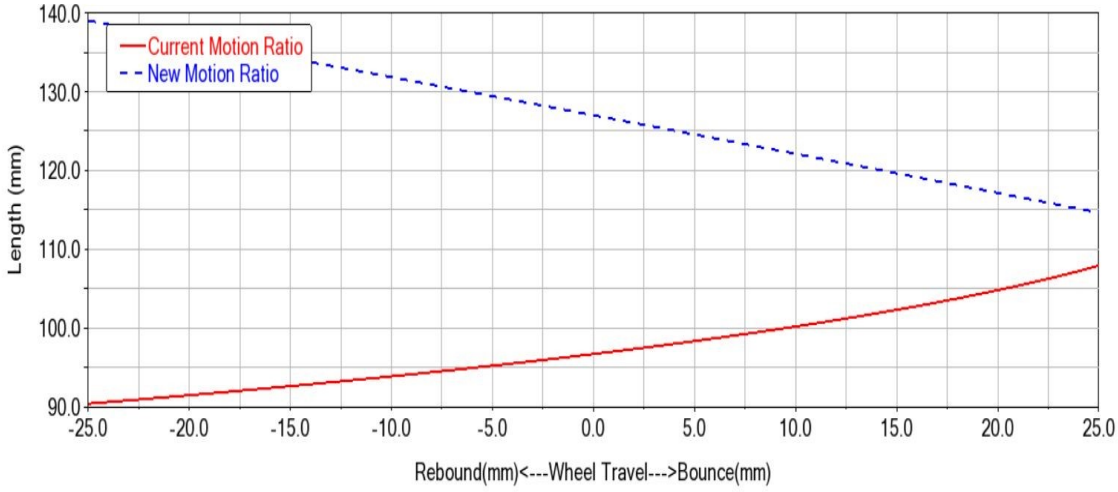

Fig. 7.8. Motion ratio for modified front suspension system

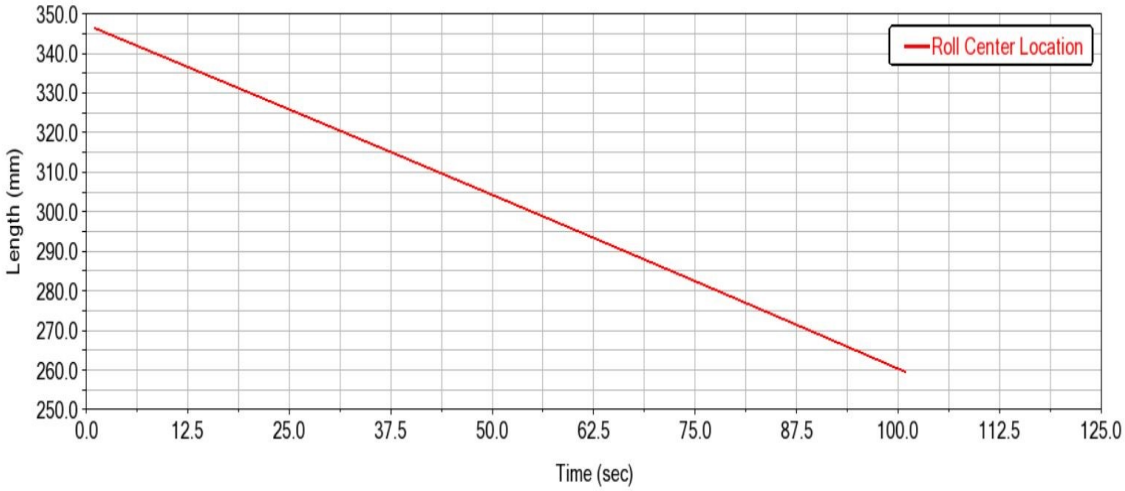

Fig. 7.9. Roll center location for modified front suspension system

what it was designed for. This is because of the roll center calculation method used by MBD model. A roll center is a imaginary point which when connected with the other respective roll center forms an imaginary axis across which the vehicle is expected to roll when subjected to force that is acting on its CG. A roll center and roll axis is just an estimation to under roll characteristics better. Even though the geometric

representation helps in understanding roll center height in steady conditions, a roll center is developed only during conditions of wheel movement and dynamic events. Since MBD model uses both geometric representation and kinematic equations to find the roll center, the height at 50th second or 0 mm wheel travel is higher than the designed height. But this works in our favour as we trying to decrease the h_{arm} length.

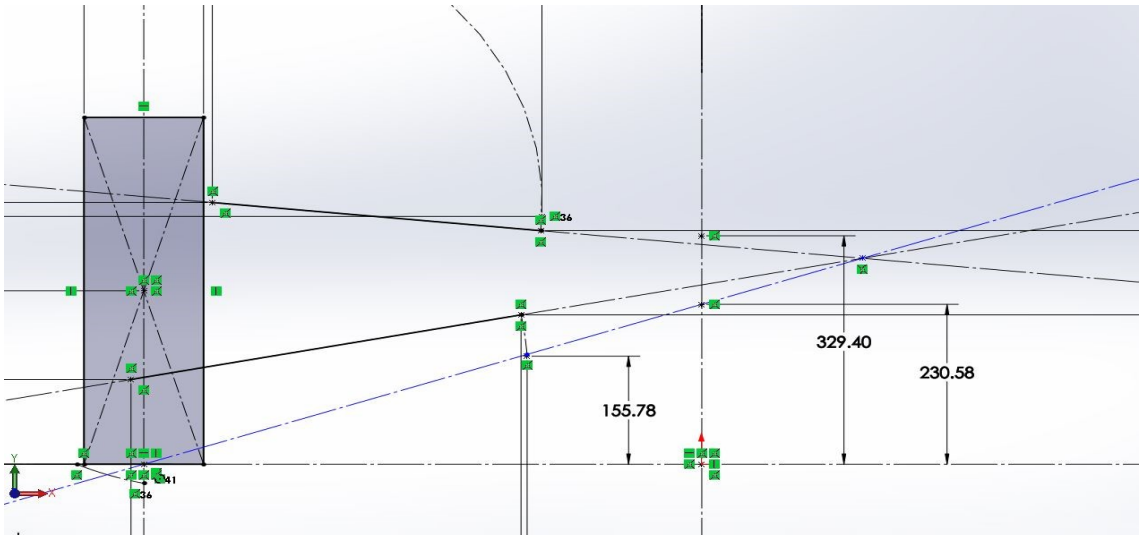

Fig. 7.10. Geometric representation of roll center

Figure 7.11 displays a comparison between the roll center of previous model named as current roll center location curve and the model under study right now named as new roll center location. The current roll center location curve starts varying from 54 mm above ground to 25 mm below ground. This makes the difference between CG height and Roll center height higher, i.e.,harm increases as time progresses. Same trend is followed by the new roll center location but the range of variation is much higher than Current roll center location curve. Thus when compared, the h_{arm} for current roll center location is higher than new roll center which increases the lateral load transfer due to body roll according to the equation mentioned in [20]. In other words, the new roll center location puts us in advantage when it comes to lateral load transfer.

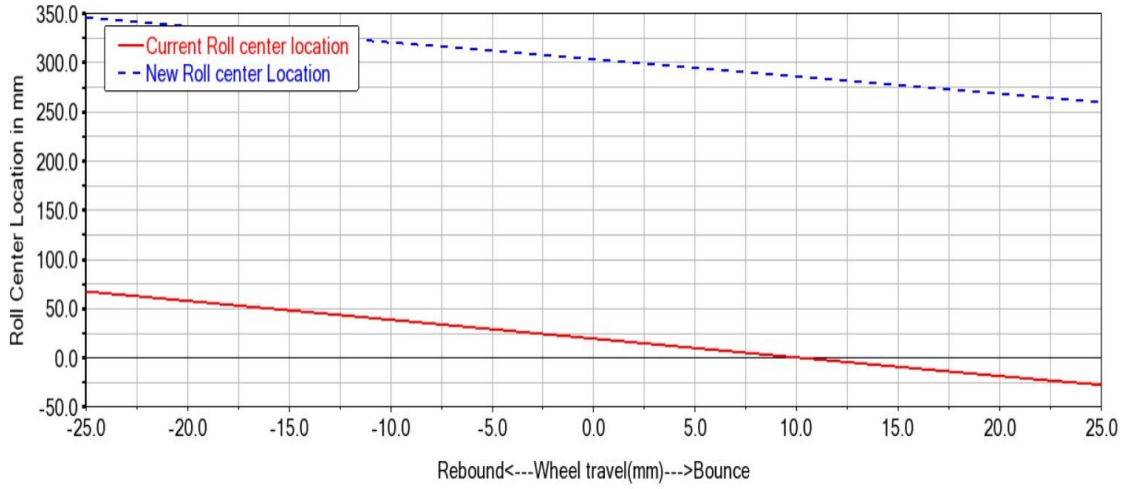

Fig. 7.11. Roll center comparison for modified front suspension system

7.2.2 Parallel wheel travel test for rear suspension system

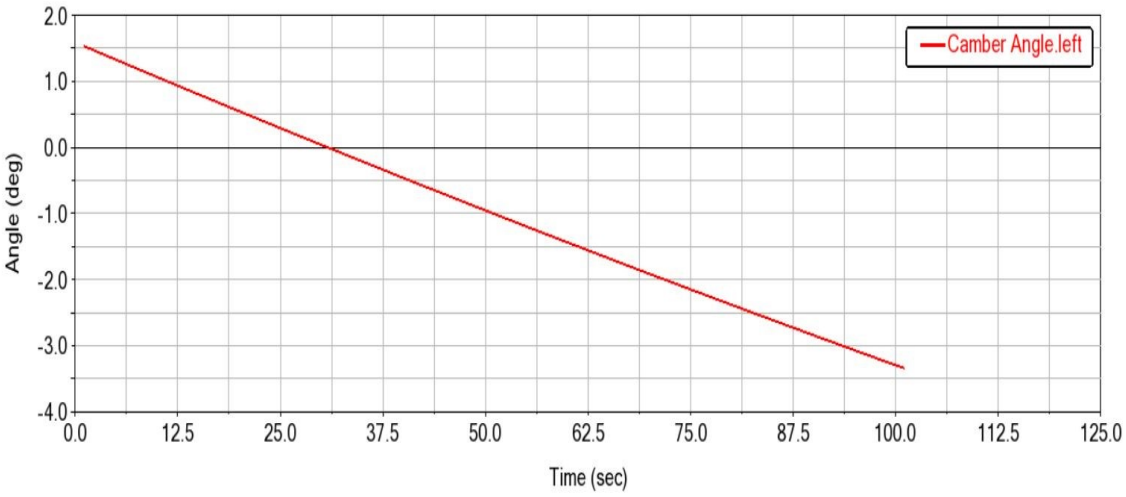

Fig. 7.12. Camber variation for modified rear suspension system

By starting with observation in the camber angle for rear suspension system, as the wheel travels from -25 mm to 25 mm, the camber angle changes from 1.5 deg to -3.4 deg. The rear wheels have been set with an offset camber angle of - 1 deg for this

testing. This offset has been selected from the comparison figure 7.13 in which the modified system is tested for varying camber angle from -1 deg to -5 deg. With the intention of losing a portion of grip in the rear tire during the event such as cornering, the offset is set to -1 deg. In figure 7.13, the x-axis is selected to be the wheel travel.

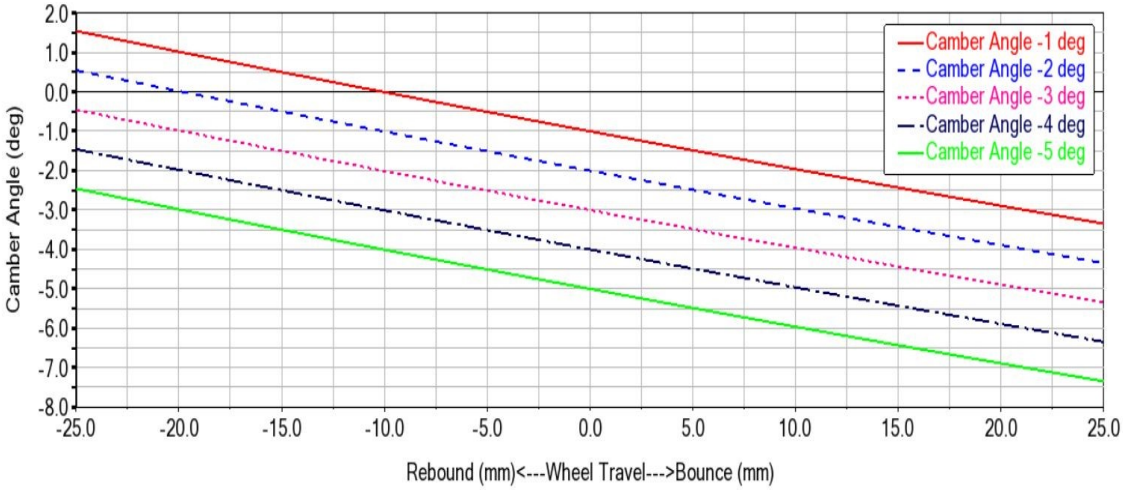

Fig. 7.13. Camber comparison for modified rear suspension system

From figure 7.13 it can be observed that the camber angle offset when set to -1 deg, tends to become positive during the event when the tire experiences camber gain. In events such as cornering, when the tire on outwards turning circle tends to gain positive camber whereas the inner tire gains negative camber. By setting the offset to -1 deg, the camber angle can go upto 1.5 deg when exposed to extreme camber gain situations. By gaining positive camber, the tire tends to lose its grip as the contact between the tire and ground decreases during positive camber. Note that the camber angle remains positive for shorter portion of wheel travel,i.e., from -25 mm to -10 mm of wheel travel. This helps the vehicle in maintaining its handling performance for majority of the portion of the test by staying negative [13].

The toe angle variation in figure 7.14 shows similar trend as in figure 4.10 with wider range of toe angle. As mentioned above the toe angle no changes are made to toe angle of the rear suspension model yet but the range is more for the variation than

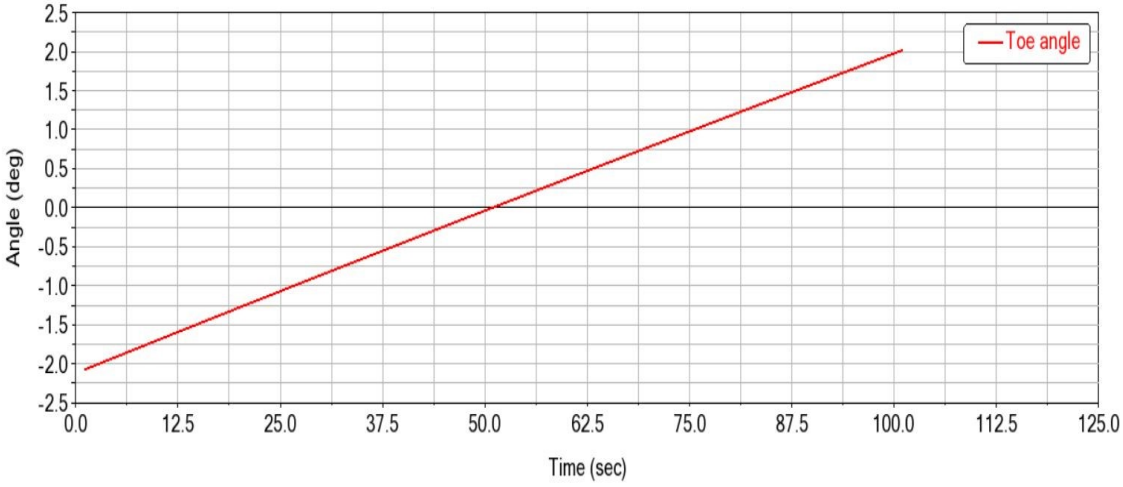

Fig. 7.14. Toe variation for modified rear suspension system

the previous model which varies within the range of 1 deg. This amount variation in range is not desired in this model especially in a rear suspension system where the tire is limited by the tie rods of fixed length. But this toe angle can be manipulated by changing tie rod lengths and can be covered in future experiments. As of now, the tire tends to lean outside when subjected to normal force or in other words when the wheel travel progresses from -25 mm to 25 mm. The toe becomes 0 deg at 51st second and varies from -2 deg to 2 deg. In this result as well the time interval on x axis is divided in more parts for accuracy of the results.

When compared to figure 4.13, the figure 7.15 shows a similar trend in the graph, but the values are far more greater in figure 7.15 as compared to figure 4.13. With the initiation of test, the force increases from 120 N and reaches its maximum force, that is, 620 N approx at around 101st second. The factor that could be contributed for the range of force shown in figure 7.15 as mentioned before could be the motion ratio of the system. This can be observed from the figure 7.16 which shows comparison of motion ratio for both previous and the one under study model.

In figure 7.16, it can be seen that the graph for both systems start from almost similar point, i.e., 180 mm and change slope as the test progresses. The graph men-

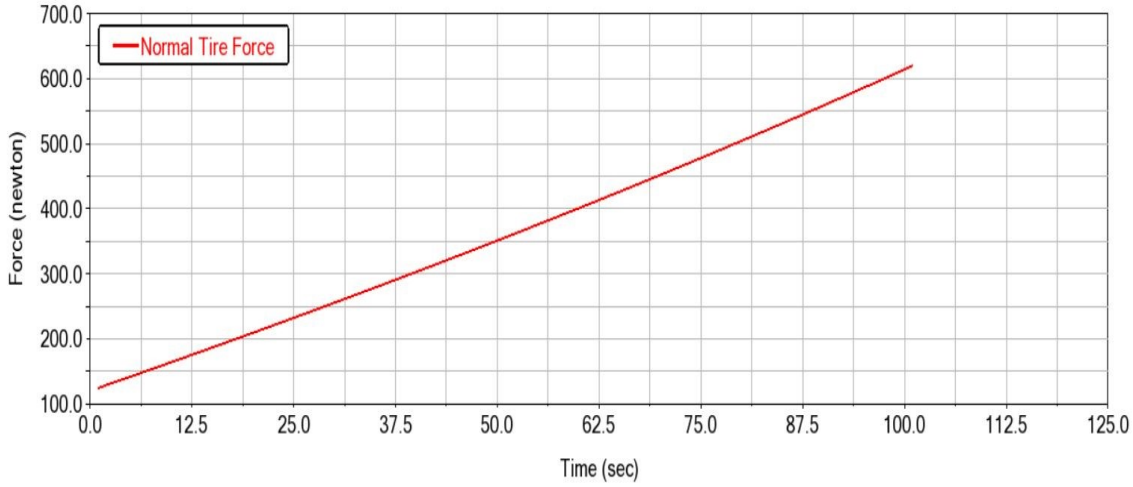

Fig. 7.15. Normal force variation for modified rear suspension system

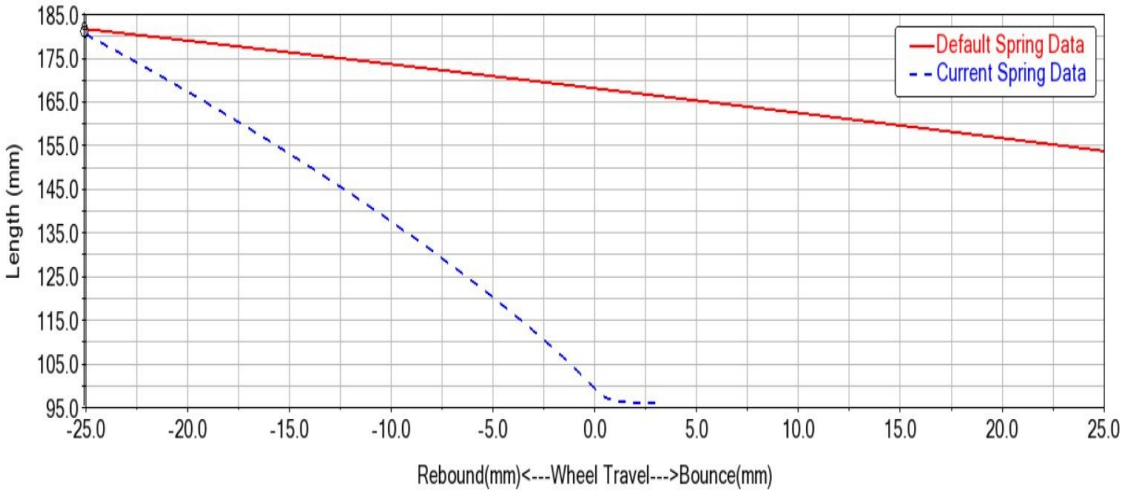

Fig. 7.16. Motion ratio comparison for modified rear suspension system

tioned as current spring data displays the previous model under study and the default spring data represents the modified version of it. The slope when calculated for the previous model graph comes to be -3.346 and for the modified model, it comes to be -0.534. From the previous graphs and this graph from figure 7.16, it can be observed that as the slope of the graph increases, the force on the wheel dampens which can

also mean that force is not being transmitted to the spring damper system. This can result in development of undesired forces and stress in the rigid elements of the vehicles including wishbones. The wishbones are naturally designed to break as a safety measure to reduce the shock that can hit the chassis and ultimately the driver [13]. As spring alignment and position plays a vital role in deciding the motion ratio of the system, the motion ratio from previous model can mean development of undesired forces in system and could be a considered as a drawback for the system.

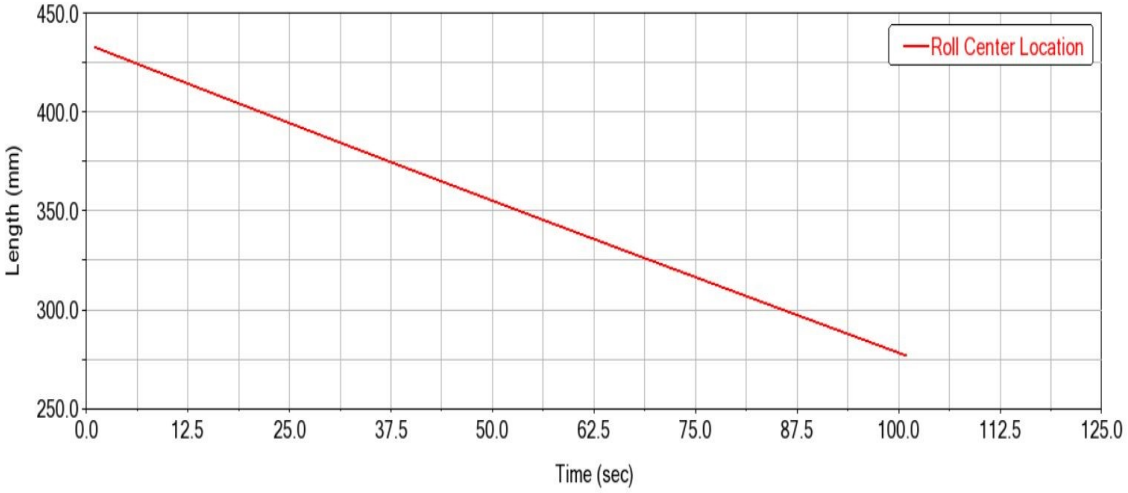

Fig. 7.17. Roll center location for modified rear suspension system

The roll center location variation and pattern is similar to the one we have seen before in the front suspension system. The graph is obvious because as per the geometry the wishbones outboard pivot points move from bottom to up as the tire moves from -25 mm to 25 mm and by doing so cause the instantaneous center to move from upwards to downwards. Thus the trend in Roll center height can be observed from 430 mm to 225 mm. The roll center height geometric representation is on same parameters as the front suspension system from figure 7.10. Thus figure 7.10 can be considered as reference for rear roll center height. In commercial vehicles the rear roll center height is more than the front roll center height and above CG height. The reason for this is it eases load transfer in the rear to help reduce understeer. The

model under study has approx 355 mm roll center height. During the test, the roll center height can go as high as 430 mm. Due to this, the h_{arm} change sign due to increase in roll center height. Since the sign changes for harm, lateral load transfer is less as the denominator becomes greater than the numerator in accordance with the equation. Below figure 7.18 gives roll center variation for previous and modified model.

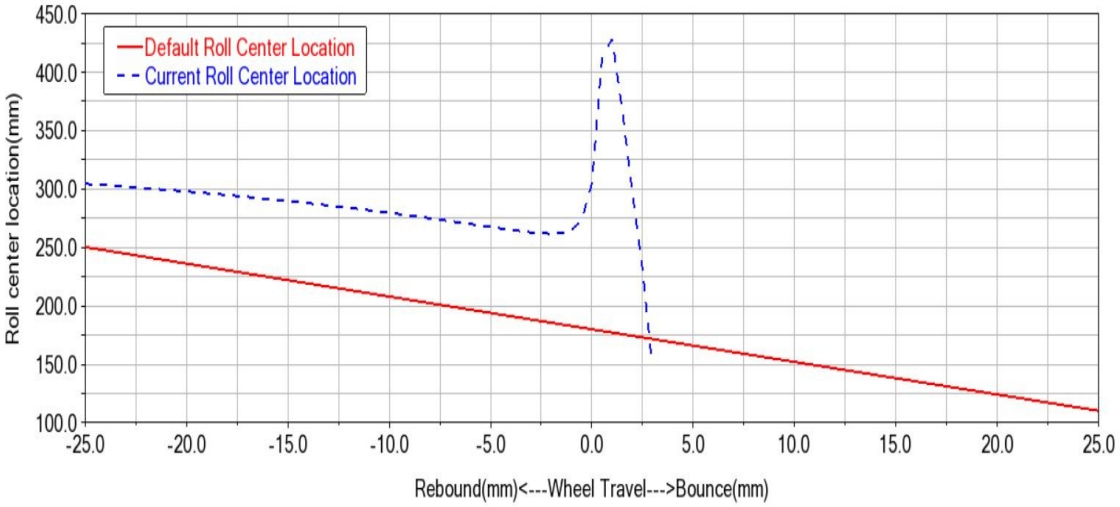

Fig. 7.18. Roll center comparison for rear suspension system

By comparing the roll center location and its variation for both models, the roll center location for previous seems to have an upper hand considering its height variation and the effect it may cause on load transfer based on the equation. But the graph shows a sudden anomaly in which the roll center height spikes up till 425 mm and comes down with steep slope. This anomaly can cause problems in handling in the vehicle if subjected to extreme conditions.

7.2.3 Skid-pad test for full vehicle assembly

As mentioned before in the explanation about skidpad test in figure, the intention of performing skid pad test is to understand maneuverability of the vehicle under

test. The test conducted for this model is completely identical with the previous test, i.e., the vehicle is given a circular path of 8 metre radius to move at a constant velocity. This test is specifically designed to understand vehicle behavior when it is rotating in a circle and with constant velocity and observe forces acting on the vehicle and how the alignment of the vehicle contributes to the performance of the vehicle in constant radius cornering events. As established from various references about constant radius cornering, the vehicle will be given a constant velocity of 20km/hr and will be compared with the results of the previous model. Initially the focus was based on change of slip angle and the intention of the study was to learn to control that change. After a lot of research it came to light that the change of slip angle is a characteristic of the tire of the vehicle. As model has limitations in the tire model used as default, it becomes way more complex to control characteristics of the tire. Thus, focus was diverted to other parameters that affect understeer and oversteer of the vehicle and those are discussed further. Duration for this test is set for 20 seconds with velocity 20km/hr throughout the test with 100 steps and constant steer angle of 30 deg. The transmission gear system is kept constant. Primary goal of this experimentation is now to reduce understeer that was observed in the first model and promote oversteer to overcome that problem.

After running the test successfully for 20 seconds at 20 km/hr the tire side slip angle for both front and rear and plotted and is represented in figure 7.20. From comparison, it can be said that the rear tire side slip angle is lower than the front tire side slip angle. The range for front slip angle starts from approx 0.02 deg and goes as high as 0.45 deg, whereas the range for rear slip angle starts from -0.1 deg to 0.1 deg. When compared to the previous model result, the side slip angle has low values in figure 7.20 which can mean that the changes in slip angle are not high and the variation is low. Even though the test is run for 20 seconds, the graph ends at approx 6.6 sec. Although the values are low for side slip angle, it is evident that the front slip angle is greater than rear. Which means that the vehicle is still experiencing understeer and the same phenomenon is observed in the animated results

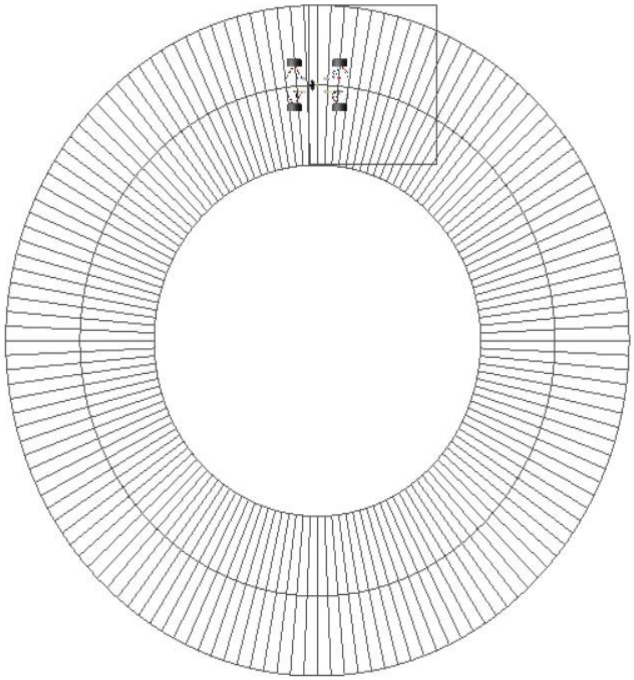

Fig. 7.19. Skid-pad test setup

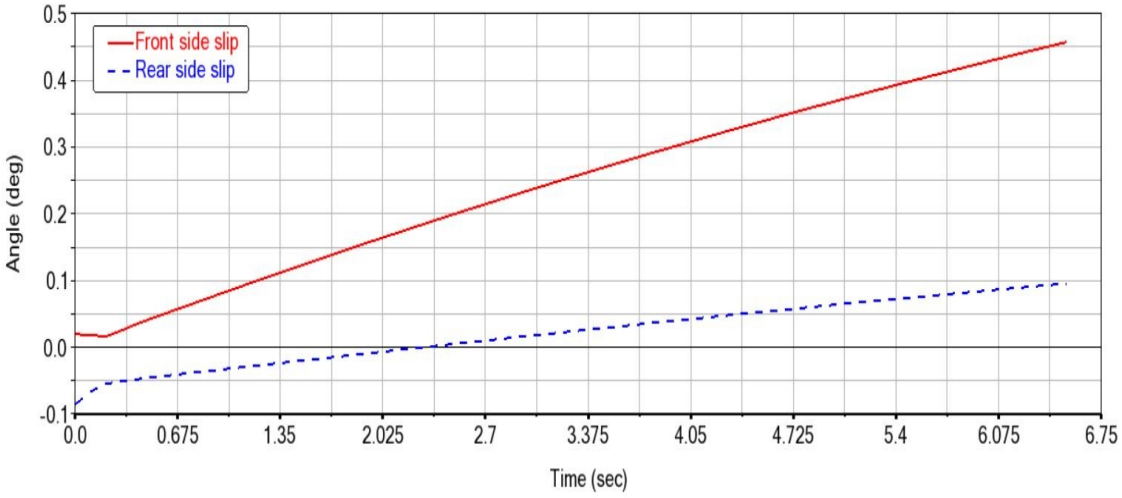

Fig. 7.20. Slip angle comparison in front and rear suspension system

when compared. The start of both curves are uneven for the first 0.5 seconds which was believed to be due to yaw rate and would decrease with decrease in yaw rate.

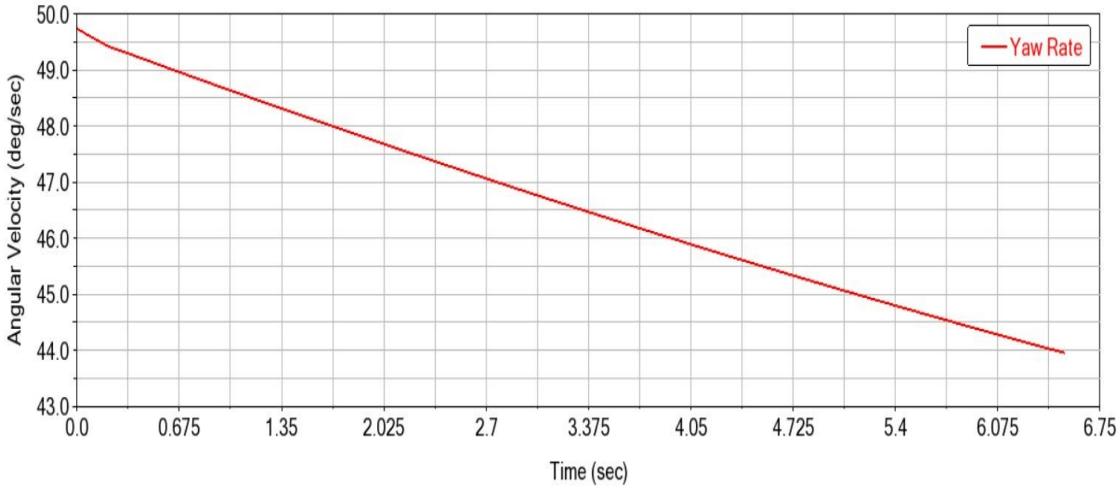

Fig. 7.21. Yaw rate for modified version of the vehicle

Even though the reason for the instability was first considered to be the yaw rate, the magnitude of yaw rate turns out to be higher than expected which rules it out for being the reason for the fluctuation in the side slip angle. Since now the magnitude and nature of yaw rate is known, the reason for the slight fluctuations at the start are now unknown and yet to be figured out. The yaw rate ranges from 49.75 deg/sec to 44 deg/sec over the time period of approx 7 seconds. As compared to the previous model, the values for this model for yaw rate are higher which can again be considered as a drawback in the model.

From figure 7.20 and 7.21, the experiment seemed a failure until its frames were compared. The animated frames are used to study the path of the vehicle and comes handy when you have to observe the exact location from where it started deviating from its path. represents one such attempt. In the above figure 7.22 the frames from left are from the previous model and on the right is the modified model. When compared, the vehicle model on the left seems to deviate from its path as it reaches half the path of the circle. Whereas, on right, the modified model also tends to go out

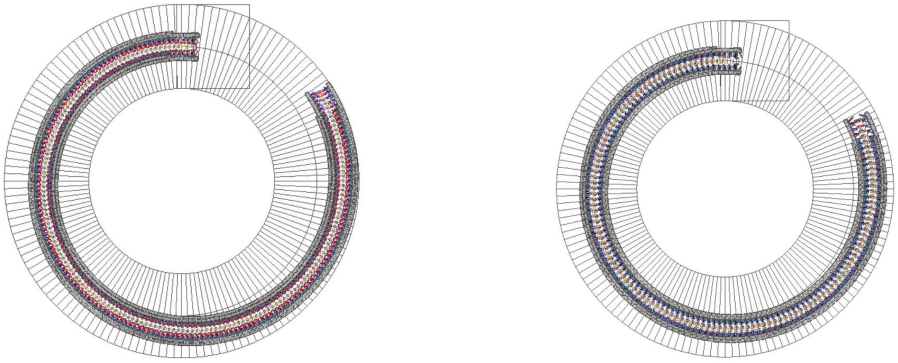

(a) Current vehicle (b) Modified vehicle

Fig. 7.22. Skidpad test comparison

of path but the deviation is delayed in the model. Although the results for tire side slip angle in figure 7.20 are in favor of understeer condition, the range of variation of tire side slip angle is lower as compared to the previous model. Even in figure 7.23, the lateral load transfer in front is way more than the rear. Even though the load transfer follows the equation under study, the intention of achieving higher load transfer in the rear as compared to the front is negated which can be said from figure 7.23. Even after the delay deviation, deviation does take place inevitably and the results from figure 7.20, 7.21 and 7.23 do point towards it. This delay in deviation could be attributed to the attempt of modifying the geometry to increase the roll center height in front, thus, making it more stiffer than the rear system.

As mentioned in figure 7.23, the lateral load transfer in front is much higher than the rear load transfer. The front load transfer starts from around 510 kgs and reduces to 455 kgs approx. For the lateral load transfer for the rear starts from 255 kgs and reduces to 225 kgs. The slope for front load transfer is -5.2 where as for rear load transfer is -8.3. This means that the load transfer in front reduces at higher rate than the rear. This could be because of the roll center manipulation for front and rear and could be considered as a contributing factor in delay for deviation in vehicle path. But as mentioned before, the load transfer is higher in front than rear and does lead to deviation in path leading to understeer inevitably. The reasons for this understeer

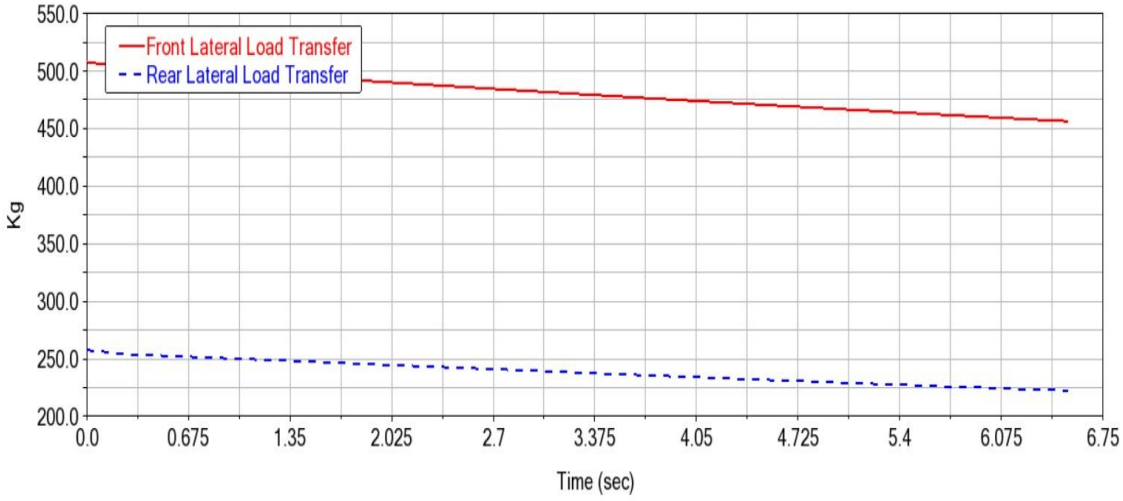

Fig. 7.23. Lateral load comparison for modified version of the vehicle

can be narrowed down to the limitations of the model and will be discussed in next chapter.

7.3 Comparison between current models with literature data

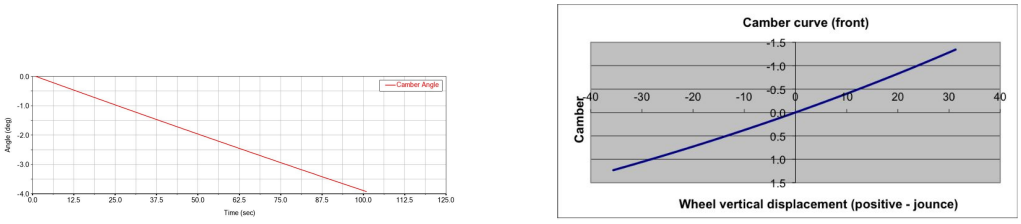

(a) modified front suspension system (b) reference

Fig. 7.24. Camber variation comparison of modified front system and reference [21]

In reference [21], the vehicle under study is FSAE vehicle representing University of Western Australia and is tested for stability analysis. In figure 8.1, the camber angle curve is represented from the vehicle under study in reference [21]. As can be observed in the figure 8.1, the the camber angle curve is tested for wheel travel of

40 mm rebound and 40 mm bump. The camber angle varies from 1.4 to -1.4 deg. By comparing camber angle variation in figure 7.4 and 8.1, it can be observed both the graphs are linear in nature. In figure 7.4, the graph decreases linearly whereas in figure 8.1, the graph increases linearly going from positive camber to negative camber. The values in both figures are completely different as the camber curve varies from -1.4 to 1.4 in figure 8.1 and from 0 deg to -3.8 deg in figure 7.4. This change can be attributed to the difference in the model under study. For example, in figure 7.4, the static camber is set to be -2 deg and the range of operation is 0 to -4 deg. But the figure in 8.1 the nothing specific about static camber is mentioned which could mean that the model is operated at neutral, i.e., at 0 deg for the test.

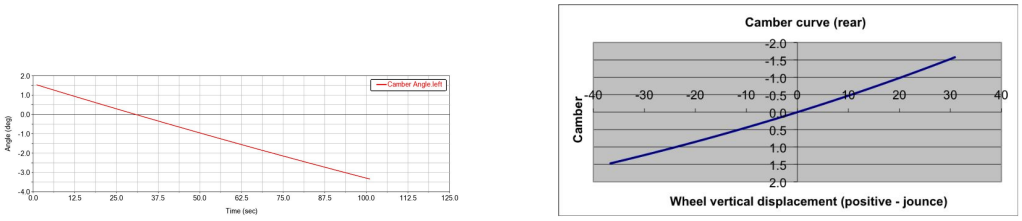

(a) modified rear suspension system (b) reference

Fig. 7.25. Camber variation comparison of modified rear system and reference [21]

Similar to the figure 8.1, figure 8.2 is also the camber curve but for rear suspension system of the same FSAE vehicle. The suspension system is tested for 40 mm rebound and bump and is plotted against the wheel travel. By comparing figure 7.12 with figure 8.2, the similar trend as mentioned before can be observed. In figure 7.12, the camber varies from 1.4 deg to -3.4 deg, whereas the camber variation in figure 8.2 is from 1.5 deg to -1.6 deg. Even with the difference in the values, the nature of the graph can be considered similar. The difference in values can be attributed to the model parameters and static conditions. The difference in the axis plays an important role in this comparison. As can be observed that the figure in 7.12 is against time and in figure 8.2 is against wheel travel, the graphs still can be compared as the nature shown by the graph in with respect to both time and wheel travel is the same.

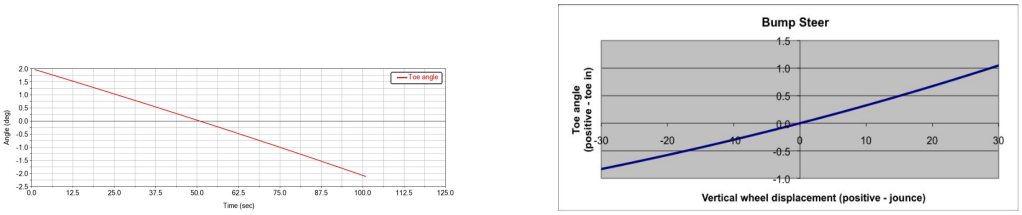

(a) modified front suspension system (b) reference

Fig. 7.26. Toe variation comparison of modified front system and reference [21]

From reference [21], figure 8.3 is used for toe angle comparison with the toe angle variation with the modified version of rear suspension system under study. Although, the graph is toe variation, the test conducted is for bump steer. When the tire is subjected to a sudden bump, the steering angle of the vehicle changes which also lead to the variation in toe angle. In graph variation, axis setup is also one of the important parameter. In figure 8.3, the y axis values change completely as the signs are interchanged in this graph. Also, the test is run for 30 mm droop and bump. Even though the test on the system is different that the test conducted, the variation gap could be used for indirect comparison for toe variation. As can be observed from figure 8.3 and figure 7.6, the range for toe angle varies a lot in the later. In reference [21], steering hardpoints were also designed to control the toe and caster angle. Thus the range for toe during bump steer is -0.7 deg to 1 deg approximate. The toe angle in figure 7.6 varies from 2 deg to -2.4 deg. More variation can make it difficult for handling but the range for figure 7.6 is less than 5 deg. But if compared in figure 7.6 and 8.3, figure 8.3 provides more accuracy in handling.

Installation ratio is one of the major parameter in this study as it compares and determines better position for spring-damper. From reference [21], the installation ratio is considered for comparison with the understudy motion ratio. The installation ratio from figure 8.4 cannot be compared with the motion ratio directly as the values on axis is different from the figure 7.11. Installation ratio is the ratio of spring travel to the wheel travel. But in this case, the motion ratio, i.e., the installation ratio is

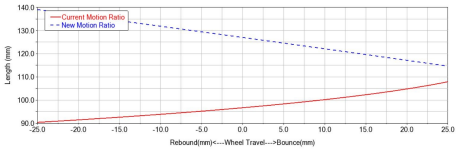

(a) modified front suspension system

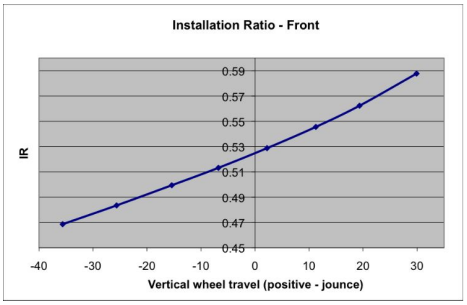

(b) reference

Fig. 7.27. Motion ratio comparison of modified front system and reference [16]

plotted against wheel travel. Also, the wheel travel for this test is 40 mm droop and 40 mm bump. When plotted spring travel vs wheel travel, the slope is considered as motion ratio. But in figure 8.4, this slope is plotted against wheel travel. If the motion ratio in figure 7.11 is scaled in similar as figure 8.4, a similar trend could be observed in the graph as the slop changes as calculated for different points succeeding the previous points. The graph ranges from 0.47 approx to 0.59 within the wheel travel of -40 mm to 40 mm. However, in figure 7.11, the spring displacement changes from 140 mm to 115 mm in length with wheel travel from -25 mm to 25 mm. Some references do use motion ratio vs wheel travel for comparison, but in our case, to compare the trend, a similar plot would be needed.

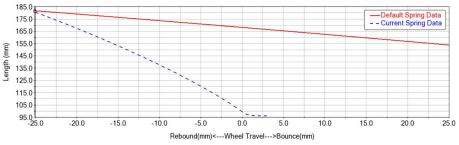

(a) modified rear suspension system

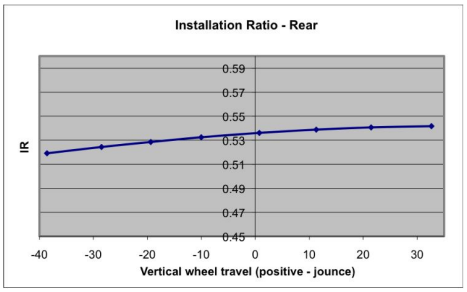

(b) reference

Fig. 7.28. Motion ratio comparison of modified rear system and reference [21]

Since the reference used is [21], the figure 8.5 is on similar lines with figure 8.4. The graph is plotted installation ratio vs wheel travel where wheel travel is from -40 mm to 40 mm. Except, figure 8.5, is installation ratio for rear suspension system and the range is different from the front suspension system. The range in this figure is narrower and the graph varies from 0.52 to 0.54. The slope in figure 7.16 varies from 185 mm to 152.5 mm approx. The slope in this figure shows similar trend as in figure 7.11. Thus the rear suspension system from reference [21], limited motion ratio trend as compared to its front. As mentioned above, the comparison of figure 7.16 with figure 8.5 is difficult even though it is indirect. With figure 8.5, the accuracy measurement would also be difficult. Thus, a reference with similar trend needs to be used for the motion ratio comparison. With figure 8.5, the accuracy measurement would also be difficult. Not that the models understudy are similar models, the values are bound to be different but even for trend comparison, the graph is difficult. Many references do use motion ratios vs wheel travel for comparison, but the graph for 7.11 and 7.16 are with different axis. So for better comparison, the reference [22] is considered where the y axis used is suspension displacement vs wheel travel.

To compare motion ratio in better way, figure 8.6 is from reference [22] is considered for comparison. By comparing figure 7.11 and 7.16 with figure 8.6, it can be observed that the y axis and x axis are different in values. In in figure 8.6, the wheel displacement varies from 0 to 14 mm in x axis, whereas, y axis is the change in length of suspension length. This is the case of providing 14 mm bump to the suspension system for both front and rear. Although the trend followed in figure 8.6 is similar to both figure 7.11 and 7.16. As the length changes when the wheel moves from negative to positive distance, i.e., from rebound to bump, the length reduces with the increase in wheel displacement. Thus, from figure 7.11 and 7.16, if the change of length is considered against wheel travel, the trend of graph would be similar to figure 8.6, i.e., linearly increasing, as the graph in 7.11 and 7.16 is linearly decreasing. The values and slope of the all three graphs can be different given the model and test conditions are not same. The wheel travel is from -25mm to 25 mm and the slope in 7.11 and

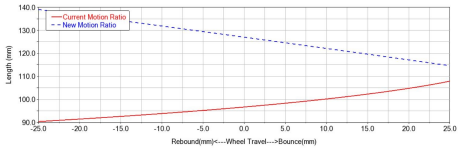

(a) Modified front

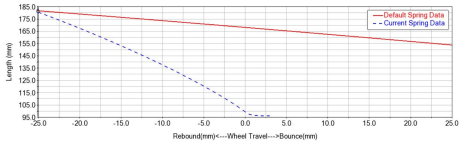

(b) Modified rear

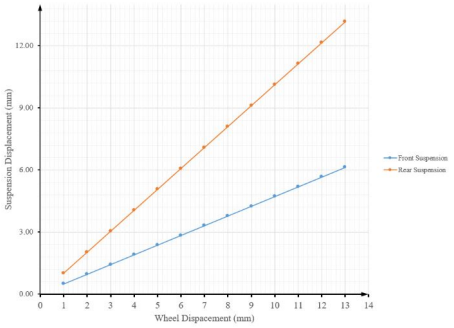

(c) reference

Fig. 7.29. Motion ratio comparison with reference [22]

7.16 is almost same, therefore, it will show graph with almost same trend in both front and rear unlike in figure 8.6, where the front slope is different than the rear slope.

Roll center location is also one of the important part of thesis. Thus, comparison with reference is important to understand how the graph in 7.9 and 7.11 varies from the reference studied. The roll center location variation in both figure 7.9 and 7.11 is linear and decreasing. In figure 7.9, it decreases from approx 345 mm to 260 mm and in figure 7.17, it decreases from 425 mm approx to 275 mm as the wheel progresses from -25 mm to 25 mm. Whereas, in figure 8.7, the wheel travels from -150 mm to 150 mm. As can be observed, the slope in rear roll center variation from 7.17 is higher than in front. Which means it varies more than the front. This is completely opposite to the trend shown in figure 8.7. In figure 8.7, front roll center variation is higher than the rear. The trend shown is an arc with does not deviate and keeps the values small with narrow range. Also the values are smaller than the ones under study. The values and shape can be attributed to the suspension model and roll

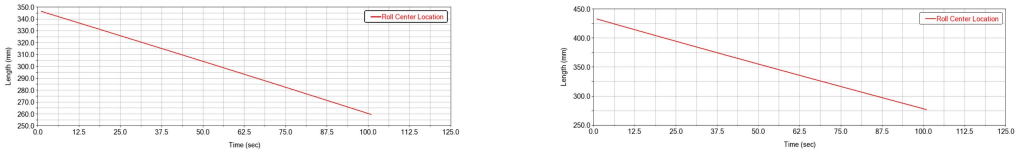

(a) Modified front (b) Modified rear

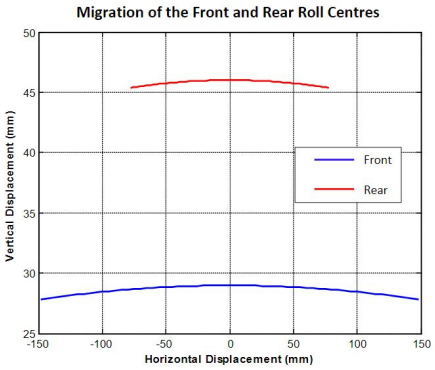

(c) reference

Fig. 7.30. Roll center location comparison with reference [23]

center requirement. Judging from the wheel displacement, the suspension type could be McPherson strut, as the reference does not mention the type of suspension being used.

8. CONCLUSION

In this thesis, the IUPUI FSAE vehicle suspension system has been studied using MBD models. The major conclusions are summarized below.

- Virtual tests on the suspension model and overall vehicle model are conducted using the MBD models. With the models, vehicle dynamics knowledge is obtained to propose a modified version of the same FSAE vehicle, which can provide better cornering performance with minimum upgrades and cost possible.

- Parallel wheel travel test is performed on suspension system in which the individual suspension system are subject to equal force on both sides to understand the variation in stability parameters such as camber angle, toe angle, motion ratio, and roll center location.

- The modified front suspension system is tested for different camber angles from -1 to -5 deg and -2 deg was selected. The toe angle varies from 2 deg to -2.2 deg with linear decreasing curve. By comparing the normal force, the graph in modified version, increases linearly from 575 N and maxes out to 1225 N. The motion ratio is -0.533. For rear suspension system, the static camber is selected to be -1 deg by comparing results from -1 deg to -5 deg. The normal force varies from 120 N to 620 N and the spring damper is position is changed for motion ratio of -0.534.

- Skid-pad test is performed on full assembly of the vehicle to understand the vehicle behavior in constant radius cornering and to study the tire side slip angle variation as it is one of the important parameters controlling alignment of the vehicle in this test.

- After obtaining the results from the tests, lateral load transfer method is used to control the vehicle slip by making changes to the geometry of the vehicle and obtaining appropriate roll center height for both front and rear suspension system.

- From results obtained, the tire side slip angle in front increases with greater slope than the tire side slip angle in rear, which means the vehicle still experiences under steer. Although, the vehicle experiences understeer, the deviation seems to have delayed in modified version when the path of both versions is compared. The lateral load transfer in front decreases with slope -5.2 whereas in rear is -8.3. The values of load transfer are higher in front than in rear which leads to the deviation in the vehicle path which can be narrowed down to the limitations of the model. By comparing results, the approach seems to delay the deviation of vehicle from its desired path, but the vehicle seems to deviate inevitably.

- This study has provided brief understanding of parameters and forces involved in suspension system and their variation in different events influencing vehicle stability.

Although the successful modeling of the FSAE vehicle in the study, there are a few limitations of the work, as described below:

- While conducting experimentation on the different systems using different boundary conditions, it could be observed that no changes could be made to the stiffness of the spring damper system of the model. Even after changing the material for the spring, the model retains its original stiffness.

- The suspension system assembly has a pushrod component that could not be removed from the model and this added up to the limitation in suspension system. By default when called upon an assembly, the pushrod comes in as default and cannot be deleted. A better position for spring and damper could be achieved with better motion ratio.

- In addition to the previous point, the anti-roll bar also is one of the components which is a default component when assembly is called. As it is essential to call in assembly as it provides a test rig for simulation, the anti-roll bar shows up with assembly being called. From different experimentation it was observed that a setting can be managed to avoid an anti-roll bar but this setting upsets the results of the experimentation whereas, when the anti-roll bar is in the system, it does not show any changes in the system. This makes its nature unpredictable in current experimentation.

- From various references, it has been observed that the tire model and its characteristics prove to be an important parameter in the cornering event. But in MBD software, the tire model used is the default rigid model and cannot be changed. Since the characteristics of tire are not known, the nature of its behavior cannot be justified. Also, since its rigid model, the default setup for constant radius cornering in software is for 61 m radius. There is a good possibility that the tire in use is designed for 61 m radius and thus, when subjected to a test with 8 m radius, the tire does not comply with it. Thus, as mentioned in results, the inevitable deviation even after the geometric change in the alignment of the vehicle could be narrowed down to this reason. Since the tire is designed for higher radius, the coefficient of friction between the tire and road could be designed for force for that radius. Since the force increases after reducing the radius, there is a possibility that the frictional force could not provide the necessary centripetal force needed to keep it from deviating. Characteristics such as coefficient of friction and stiffness of the tire could be determined because of the default model.

- Weight of the vehicle is essential for basic calculations of the statics of the vehicle. But the option for doing so is not available. This also affects the CG of the vehicle. The powertrain source manipulates the weight of the vehicle largely especially in FSAE. Software does not provide an option for selection

of powertrain or source. As an ideal IC engine can be heavier in weight, it can manipulate the CG position of the vehicle. With growing competition, the electric propulsion system and hybrid are used in FSAE competition and these powertrains are lighter in weight which also has a contributing factor in CG position.

- In addition to simulation limitations, the steer angle for the steering system is kept constant throughout the simulation. Since, steer angle can be an important factor in manipulating side slip angle, steer angle could be changed to control the side slip angle. But since this option is not available, it can be considered as a limitation for the model and its simulation.

9. CONTRIBUTION OF THE THESIS WORK

- Front suspension and rear suspension MBD models are created and show variation in suspension parameters when subject to normal force. Combined effect of front suspension system and rear suspension system is studied to understand handling effect of the vehicle.
- Lateral load transfer method is used to control the handling behavior of the vehicle. The front suspension is modified to increase stiffness and the rear suspension is modified to increase its compliance to promote oversteer.
- Position of spring-damper is manipulated to increase efficiency of spring and increase absorption of forces.

REFERENCES

REFERENCES

[1] T. Larsson, "Multibody dynamic simulation in product development," Ph.D. dissertation, Luleå University of Technology, 2001.

[2] P. Song, "Modeling, analysis and simulation of multibody systems with contact and friction," Ph.D. dissertation, University of Pennsylvania, 2002.

[3] S. Biswal, A. Prasanth, R. Udayakumar, S. Deva, and A. Gupta, "Design of a suspension system and determining suspension parameters of a medium downforce small formula type car," in *MATEC Web of Conferences*, vol. 124. EDP Sciences, 2017, p. 07006.

[4] X. Liu, J. Luo, Y. Wang, H. Guo, and X. Wang, "Analysis for suspension hardpoint of formula sae car based on correlation theory," *Research Journal of Applied Sciences, Engineering and Technology*, vol. 6, no. 24, pp. 4569–4574, 2013.

[5] R. S. Nikhil Anand, Anmol Sethi, "Suspension optimization of student formula race car," *International Journal of Aerospace and Mechanical Engineering*, vol. 1, 2014.

[6] Y. Samant Saurabh, S. Kumar, K. K. Jain, S. K. Behera, D. Gandhi, S. Raghavendra, and K. Kalita, "Design of suspension system for formula student race car," *Procedia Engineering*, vol. 144, pp. 1138–1149, 2016.

[7] W.-S. Yoo, S.-S. Kim, T.-W. Park, D.-S. Bae, and J.-H. Choi, "Multibody dynamics research in korea," *JSME International Journal Series C Mechanical Systems, Machine Elements and Manufacturing*, vol. 46, no. 2, pp. 449–458, 2003.

[8] A. Dhakar and R. Ranjan, "Force calculation in upright of a fsae race car," *International Journal of Mechanical Engineering and Tecnology (IJMET)*, 2016.

[9] S. Solmaz, M. Akar, and R. Shorten, "Center of gravity estimation and rollover prevention using multiple models & controllers," 2008.

[10] S. Chepkasov, G. Markin, and A. Akulova, "Suspension kinematics study of the" formula sae" sports car," *Procedia Engineering*, no. 150, pp. 1280–1286, 2016.

[11] L. Sun, Z. Deng, and Q. Zhang, "Design and strength analysis of fsae suspension," *The Open Mechanical Engineering Journal*, vol. 8, no. 1, 2014.

[12] I. N. Karlsson, "Design of a suspension system for a formula student race car," Ph.D. dissertation, 2018.

[13] T. Pashley, *How to build motorcycle-engined racing cars.* Veloce Publishing Ltd, 2008.

[14] J. Sebastian, S. Siyad, S. A. Jose, T. Devasia, and S. Thomas, "Concept of moving centre of gravity for improved directional stability for automobiles-simulation," *International Journal for Innovative Research in Science & Technology*, vol. 2, no. 11, 2016.

[15] A. A. Vadhe, "Design and optimization of formula sae suspension system," 2018.

[16] U. Kiencke and L. Nielsen, *Automotive control systems: for engine, driveline, and vehicle*. IOP Publishing, 2000.

[17] H. F. Grip, L. Imsland, T. A. Johansen, J. C. Kalkkuhl, and A. Suissa, "Vehicle sideslip estimation," *IEEE control systems magazine*, vol. 29, no. 5, pp. 36–52, 2009.

[18] R. Rajamani, *Vehicle dynamics and control*. Springer Science & Business Media, 2011.

[19] A. Diaz, "Fsae 2015 chassis and suspension 25% report," Bachelor's thesis, Florida International University, 2014.

[20] Skill-Lync, "Suspension design," (2018), retrieved December 2019. [Online]. Available: https://courses.skill-lync.com/courses

[21] M. Kiszko, "Rev 2011 formula sae electric," Bachelor's thesis, University of Western Australia, 2011.

[22] J. W. Wirawan, Ubaidillah, R. Aditra, R. Alnursyah, R. A. Rahman, and S. I. Cahyono, "Design analysis of formula student race car suspension system," in *AIP Conference Proceedings*, vol. 1931, no. 1. AIP Publishing LLC, 2018, p. 030051.

[23] J. Farrington, "Redesign of an fsae race car's steering and suspension system," Bachelor's thesis, University of Southern Queensland, 2011.

PUBLICATION

PUBLICATION

Publications

1. Swapnil Bansode, Drew Haywood, Marc Poynter, Marc Lind, Cody Turner, Michael Golub, Tejesh C Dube, and Jing Zhang, Modifying Exhaust and ECU for snowmobile, SAE Clean Snowmobile Challenge, MI, USA.

Poster Presentations

1. Swapnil P. Bansode, Michael Golub, Jing Zhang, 'Multi-body dynamics in FSAE vehicles', Indiana Summit 2019, Indianapolis IN; October 2019
2. Swapnil P. Bansode, Michael Golub, Jing Zhang, 'Multi-body dynamics in FSAE vehicles', IUPUI Research day 2019, Indianapolis IN; April 2019
3. Swapnil P. Bansode, Michael Golub, Jing Zhang, 'Multi-body dynamics in FSAE vehicle', ASM Indianapolis Chapter Spring Conference, Columbus, IN; February 2019.
4. Swapnil P. Bansode, Drew Haywood, Marc Poynter, Marc Lind, Cody Turner, Michael Golub, and Jing Zhang, 'Modifying Exhaust and ECU for Snowmobile', IUPUI Research Day, Indianapolis IN; April 2018